

EFFECTS OF BEAM TYPES IN THE PERFORMANCE OF FREE SPACE OPTICS
SYSTEMS

A THESIS SUBMITTED TO
THE GRADUATE SCHOOL OF NATURAL AND APPLIED SCIENCES
OF
ÇANKAYA UNIVERSITY

BY
DENİZ TATGIN


IN PARTIAL FULFILLMENT OF THE REQUIREMENTS
FOR
THE DEGREE OF MASTER OF SCIENCE
IN
THE DEPARTMENT OF ELECTRONIC AND COMMUNICATION ENGINEERING

SEPTEMBER 2008

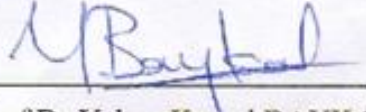
Title of the Thesis :Effects Of Beam Types In The Performance Of Free Space Optics Systems

Submitted by Deniz TATGIN

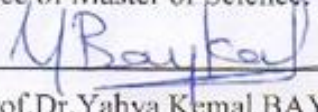
Approval of the Graduate School of Natural and Applied Sciences, Çankaya University


Prof.Dr. Yahya Kemal BAYKAL
Acting Director

I certify that this thesis satisfies all the requirements as a thesis for the degree of Master of Science.


Prof.Dr. Yahya Kemal BAYKAL
Head of Department

This is to certify that we have read this thesis and that in our opinion it is fully adequate, in scope and quality, as a thesis for the degree of Master of Science.

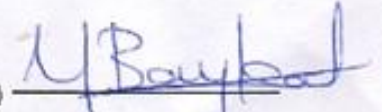

Prof.Dr. Yahya Kemal BAYKAL
Supervisor

Examination Date : 19.09.2008

Examining Committee Members

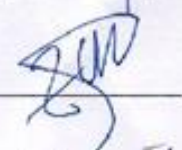
Prof. Dr. Yahya Kemal BAYKAL

(Çankaya Univ.)



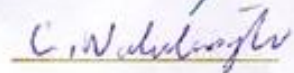
Assoc. Prof. Dr. Halil T. EYYUBOĞLU

(Çankaya Univ.)



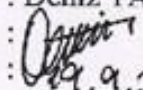
Asst. Prof. Dr. Cem NAKİBOĞLU

(Gazi Univ.)



STATEMENT OF NON-PLAGIARISM PAGE

I hereby declare that all information in this document has been obtained and presented in accordance with academic rules and ethical conduct. I also declare that, as required by these rules and conduct, I have fully cited and referenced all material and results that are not original to this work.

Name, Last Name : Deniz TATGIN
Signature : 
Date : 09.9.2008

ABSTRACT

EFFECTS OF BEAM TYPES IN THE PERFORMANCE OF FREE SPACE OPTICS SYSTEMS

TATGIN, Deniz

M.S.c., Department of Electronic and Communication Engineering

Supervisor : Prof. Dr. Yahya Kemal BAYKAL

September 2008, 98 pages

In this thesis, a general light source beam formula is developed which combines many beam types. Using different parameter sets in the general source beam formula, we obtained different beam's source equations. Using Matlab, intensity distributions at the source plane for various beam types are plotted. Received average intensity in atmospheric turbulence is calculated for the general source beam and numerical evaluations are made and the received average intensities are plotted for certain specific beams such as Dark Hollow, Flat-topped, Bottle, Lorentz and Super Gaussian beams.

Keywords: Free Space Optics, Intensity Distribution, Atmospheric Turbulence

ÖZ

IŞIK HÜZMESİ TİPLERİNİN SERBEST UZAY OPTİK SİSTEMLERİ PERFORMANSINDAKİ ETKİSİ

TATGIN, Deniz

Yükseklisans, Elektronik ve Haberleşme Mühendisliği Anabilim Dalı

Tez Yöneticisi: Prof. Dr. Yahya Kemal BAYKAL

Eylül 2008, 98 sayfa

Bu tezde, birçok hüzme tipini birleştiren bir genel ışık kaynağı formülü geliştirildi. Genel kaynak ışık hüzmesi formülünde farklı parametre setleri kullanılarak, farklı ışık hüzmelerinin kaynak denklemleri elde edildi. Matlab kullanılarak, çeşitli hüzme tipleri için kaynak düzleminde ışık şiddeti dağılımları çizildi. Genel kaynak hüzmesi için türbülanslı atmosferde alıcıdaki ortalama ışık şiddeti hesaplandı ve Dark Hollow, Flat-topped, Bottle, Lorentz ve Süper Gauss gibi bazı spesifik hüzmelerin alıcı düzleminde oluşturduğu ışık şiddeti dağılımları nümerik hesaplanarak çizdirildi.

Anahtar Kelimeler: Serbest Uzay Optik, Işık Şiddeti Dağılımı, Atmosfer Türbülansı

ACKNOWLEDGMENTS

I would like to express my sincere appreciation and gratitude to my supervisor Prof. Dr. Yahya Kemal BAYKAL for his guidance, advice, criticism, encouragements and insight throughout the research.

I would like to thank Assoc. Prof. Dr. Halil Taner EYYUBOGLU, Instructor Dr.Serap ALTAY ARPALI and Res. Asst. Canan YAZICIOĞLU for their support.

I would like to thank my son Ceyhun Uras TATGIN and my husband Fatih Güray TATGIN for their patient.

TABLE OF CONTENTS

STATEMENT OF NON PLAGIARISM	iii
ABSTRACT.....	iv
ÖZ.....	v
ACKNOWLEDGMENTS.....	vi
TABLE OF CONTENTS.....	vii
CHAPTERS:	
1. INTRODUCTION.....	1
1.1 Objectives of the Study.....	1
1.2 Organization of the Thesis.....	1
2. FSO BACKGROUND.....	3
3. ATMOSPHERIC EFFECTS ON LASER BEAM PROPAGATION.....	6
3.1 Atmospheric Attenuation.....	6
3.1.1 Absortion.....	6
3.1.2 Scattering.....	7
3.2 Atmospheric Fluctuation.....	8
3.3 The Extended Huygens-Fresnel Principle.....	9
4. GENERATING DIFFERENT BEAM'S SOURCE EQUATION FROM GENERAL SOURCE BEAM FORMULA	11
4.1 Limiting Cases.....	12

4.1.1	Bessel Beam.....	12
4.1.2	Bessel Gaussian Beam.....	15
4.1.3	Laguerre Beam.....	16
4.1.4	Laguerre Gaussian Beam.....	17
4.1.5	Dark Hollow Beam.....	21
4.1.6	Bottle Beam.....	22
4.1.7	Flat-topped Beam.....	24
4.1.8	Super Gaussian Beam.....	26
4.1.9	Lorentz Beam.....	28
5.	NUMERIC CALCULATION OF AVERAGE RECEIVED INTENSITY BY USING GENERAL BEAM FORMULA.....	30
5.1	Dark Hollow Beam.....	33
5.2	Flat-topped Beam.....	35
5.3	Bottle Beam.....	37
5.4	Lorentz Beam.....	43
5.5	Super Gaussian Beam.....	47
6.	CONCLUSIONS.....	53
	REFERENCES.....	R1
APPENDIX:		
A.	MATLAB PROGRAM USED IN THESIS.....	A1

LIST OF TABLES

TABLES

Table 2.1: Properties of terrestrial FSO and RF communications.....	5
---	---

GCPRIS

LIST OF FIGURES

FIGURES

Figure 3.1: Laser beam wander due to turbulence cells which are larger than the beam diameter.....	8
Figure 3.2: Scintillation or fluctuations in beam intensity at the receiver due to turbulent cells that are smaller than the beam diameter.....	9
Figure 4.1: Intensity distribution of Bessel beam at the source plane.....	15
Figure 4.2: Intensity distribution of Laguerre Gaussian beam at the source plane with mode orders (1,2).....	19
Figure 4.3: Intensity distribution of Laguerre Gaussian beam at the source plane with mode orders (2,3).....	19
Figure 4.4: Intensity distribution of Laguerre Gaussian beam at the source plane with mode orders (0,5).....	20
Figure 4.5: Intensity distribution of Laguerre Gaussian beam at the source plane with mode orders (1,10).....	20
Figure 4.6: Intensity distribution of dark hollow beam at the source plane.....	22
Figure 4.7: Bottle beam intensity at the source plane.....	23

Figure 4.8: Flat-topped intensity at the source plane with $N_f = 8$ 25

Figure 4.9: Flat-topped intensity at the source plane with $N_f = 5$ 25

Figure 4.10: Super Gaussian beam intensity at the source plane for $N_s = 8$ 27

Figure 4.11: Super Gaussian beam intensity at the source plane for $N_s = 2$ 27

Figure 4.12: Lorentz beam intensity at the source plane.....29

Figure 5.1: The normalized average intensity of circular dark hollow beam at several propagation distances in a turbulent atmosphere with $C_n^2 = 10^{-15} m^{-2/3}$, $w_o = 2\text{cm}$, $N=3$, $p=9$, $\lambda = 632.8\text{nm}$34

Figure 5.2: The normalized average intensity of circular dark hollow beam at several propagation distances in a turbulent atmosphere with $C_n^2 = 10^{-14} m^{-2/3}$, $w_o = 2\text{cm}$, $N=3$, $p=9$, $\lambda = 632.8\text{nm}$35

Figure 5.3: The normalized average intensity of circular flat-topped beam at several propagation distances in a turbulent atmosphere with $C_n^2 = 10^{-15} m^{-2/3}$, $w_o = 2\text{cm}$, $N_f = 8$, $\lambda = 632.8\text{nm}$36

Figure 5.4: The normalized average intensity of circular flat-topped beam at several propagation distances in a turbulent atmosphere with $C_n^2 = 10^{-14} m^{-2/3}$, $w_o = 2\text{cm}$, $N_f = 8$, $\lambda = 632.8\text{nm}$37

Figure 5.5: The normalized average intensity of circular bottle beam at several propagation distances in a turbulent atmosphere with

$C_n^2=10^{-15} m^{-2/3}$, $w_o=2\text{cm}$, $\lambda =632.8\text{nm}$39

Figure 5.6: The normalized average intensity of circular bottle beam at several propagation distances in a turbulent atmosphere with $C_n^2=10^{-14} m^{-2/3}$, $w_o=2\text{cm}$, $\lambda =632.8\text{nm}$40

Figure 5.7: The normalized average intensity of circular bottle beam at several propagation distances in a turbulent atmosphere with $C_n^2=10^{-14} m^{-2/3}$, $w_o=2\text{cm}$, $\lambda =1.55 \mu \text{m}$41

Figure 5.8: The normalized average intensity of circular bottle beam at several propagation distances in a turbulent atmosphere with $C_n^2=10^{-14} m^{-2/3}$, $w_o=4\text{cm}$, $\lambda =632.8\text{nm}$42

Figure 5.9: The normalized average intensity of lorentz beam at several propagation distances in a turbulent atmosphere with $C_n^2=10^{-15} m^{-2/3}$, $w_o=2\text{cm}$, $\lambda =632.8\text{nm}$44

Figure 5.10: The normalized average intensity of lorentz beam at several propagation distances in a turbulent atmosphere with $C_n^2=10^{-14} m^{-2/3}$, $w_o=2\text{cm}$, $\lambda =632.8\text{nm}$45

Figure 5.11: The normalized average intensity of lorentz beam at several propagation distances in a turbulent atmosphere with $C_n^2=10^{-14} m^{-2/3}$, $w_o=2\text{cm}$, $\lambda =1.55 \mu \text{m}$46

Figure 5.12: The normalized average intensity of lorentz beam at several propagation distances in a turbulent atmosphere with $C_n^2=10^{-14} m^{-2/3}$, $w_o=4\text{cm}$, $\lambda =632.8\text{nm}$47

Figure 5.13: The normalized average intensity of Super gaussian beam at several propagation distances in a turbulent atmosphere with $C_n^2=10^{-15} m^{-2/3}$, $w_o=2\text{cm}$ $\lambda=632.8\text{nm}$49

Figure 5.14: The normalized average intensity of Super gaussian beam at several propagation distances in a turbulent atmosphere with $C_n^2=10^{-14} m^{-2/3}$, $w_o=2\text{cm}$, $\lambda=632.8\text{nm}$50

Figure 5.15: The normalized average intensity of Super gaussian beam at several propagation distances in a turbulent atmosphere with $C_n^2=10^{-14} m^{-2/3}$, $w_o=2\text{cm}$, $\lambda=1.55 \mu \text{m}$51

Figure 5.16: The normalized average intensity of Super gaussian beam at several propagation distances in a turbulent atmosphere with $C_n^2=10^{-14} m^{-2/3}$, $w_o=4\text{cm}$, $\lambda=632.8\text{nm}$52

LIST OF ABBREVIATION

ABBREVIATION

DHB:..DARK HOLLOW BEAM

FSO:..FREE SPACE OPTICS

GCPRIS

CHAPTER 1

INTRODUCTION

Free-Space Optics (also known as “FSO”, “Wireless Optics” or “Optical Wireless”) is an optical data, voice and video transmission system. Like fiber optics cable, wireless optics communication systems use laser light to transmit a digital signal between two transceivers. However, unlike fiber, the laser light is transmitted through air (free-space) instead of through a glass strand. In order for the digital signal to be transmitted and received, there must be clear line of site between each wireless optics unit. In other words, there should be no obstructions such as trees or buildings between the transceiver units. FSO is primarily deployed where performance, security, rapid deployment, and cost-savings are critical issues [1].

1.1 Objectives of the Study

It is the aim of this work to combine the existing optical beam fields in a single general beam formula, plot the intensity distributions at the exit plane of the laser and investigate the propagation characteristics at different distances in atmospheric turbulence by numerical calculation.

1.2 Organization of the Thesis

This thesis comprises six chapters. Chapter 1 is an introduction to this study which contains the objective of this thesis.

Chapter 2 includes some basic information about Free Space Optics.

In Chapter 3 the atmospheric effects on laser beam propagation are introduced.

In Chapter 4 the existing optical beam fields such as Bessel, Bessel Gaussian, Laguerre, Laguerre Gaussian, Dark Hollow, Bottle, Super Gaussian, Lorentz and flat-topped beams are combined in a single general source beam formulation and source intensity distributions are plotted via Matlab code.

In Chapter 5 general source beam formulation and Matlab code are used to find the numerical calculation of the average received intensity of various beam types in turbulence.

The thesis is finalized with the conclusion in Chapter 6.

CHAPTER 2

FSO BACKGROUND

The concept of optical wireless communications has been used for millennia, examples including smoke signals and semaphore flags. In 1880, Alexander Graham Bell patented the photophone, which modulated light reflected from the sun with a voice signal and transmitted that across free space to a solid state detector. Thus was born the first Free Space Optics (FSO) link. Given that Bell described the photophone as “the greatest invention I have ever made; greater than the telephone,” we can see that the hype for FSO is also nothing new. Unfortunately, the weather availability of the photophone was less than 50%, as it required direct sunlight for operation [2].

FSO transmits infrared, eye-safe light beams from one "telescope" to another using low power infrared lasers in the terahertz spectrum. The beams of light in FSO systems are transmitted by laser light focused on highly sensitive photon detector receivers. These receivers are telescopic lenses able to collect the photon stream and transmit digital data containing a mix of internet messages, video images, radio signals or computer files. Commercially available systems offer capacities in the range of 100 Mbps to 2.5 Gbps, and demonstration systems report data rates as high as 160 Gbps.

FSO systems can function over distances of several kilometers. As long as there is a clear line of sight between the source and the destination and enough transmitter power, FSO communication is possible.

Unlike radio and microwave systems, FSO is an optical technology and no spectrum licensing or frequency coordination with other users is required, interference from or to other systems or equipment is not a concern, and the point-to-point laser signal is extremely difficult to intercept, and therefore secure. Data rates comparable to optical fiber transmission can be carried by FSO systems with very low error rates, while the extremely narrow laser beam widths ensure that there is almost no practical limit to the number of separate FSO links that can be installed in a given location.

FSO systems offer a flexible networking solution that can offer broadband solutions. Only FSO provides the essential combination of qualities required to bring the traffic to the optical fiber backbone – virtually unlimited bandwidth, low cost, ease and speed of deployment. Freedom from licensing and regulation translates into ease, speed and low cost of deployment.

Since FSO optical wireless transceivers can transmit and receive through windows, it is possible to mount FSO systems inside buildings, reducing the need to compete for roof space, simplifying wiring and cabling, and permitting the equipment to operate in a very favorable environment. The only essential point to be fulfilled for FSO is line of sight between the two ends of the link.

The advantages of FSO do not come without some cost. When light is transmitted through optical fiber, transmission integrity is quite predictable – barring unforeseen events such as backhoes or animal interference. When light is transmitted through the air, as with FSO optical wireless systems, it must cooperate with a a complex and not always quantifiable subject - the atmosphere [3].

FSO technology also emerged as a key technology for the development of rapidly deployable, secure communication and surveillance systems, which can cooperate with other technologies to provide a robust, advanced sensor communication network. However, the line of sight requirement for optical links reduces flexibility in forming FSO communication networks. Compared with broadcast radio frequency (RF) networks, FSO networks do not have an obvious simple ability to distribute

data and control information within the network. Table 2.1 summarizes the difference between FSO and RF technologies.

Table 2.1: Properties of terrestrial FSO and RF communications.

	FSO Links	RF Links
Typical Data Rate	100 Mbps to ~Gbps	Less than 100 Mbps [†]
Channel Security	High	Low
Component Dimension	Small	Large
Source of Signal Degradation	Atmospheric turbulence and obscuration	Multipath fading, rain, and user interferences

Hybrid FSO/RF networks combine the advantages of both systems and avoid the disadvantages of FSO or RF alone [4].

Most FSO systems use simple ON–OFF keying (OOK) as a modulation format, the same standard modulation technique that is used in digital fiberoptics systems, wherein data are typically transmitted in a digital format with light “ON” representing a “1” and light “OFF” representing a “0” [5].

Atmospheric conditions affect beams’ intensity at the receiver. The purpose of all the studies is to reduce these negative effects introduced by the atmosphere.

CHAPTER 3

ATMOSPHERIC EFFECTS ON LASER BEAM PROPAGATION

Interest in high-data-rate free-space optical (FSO) laser communication systems has grown significantly in recent years because of the advantages offered by FSO systems over radio frequency (RF) systems. Most advantages are simple consequences of the short wavelengths associated with optical waves. However, there are some drawbacks that arise from the shorter wavelengths used in FSO systems. Atmospheric factors are the most serious drawback to FSO systems. Optical turbulence resulting from small temperature variations gives rise to power losses from spreading of the beam beyond that due to diffraction alone, and to temporal and spatial fluctuations of the laser beam known as scintillation [6].

Atmospheric effects on laser beam propagation can be broken down into two categories: attenuation of the laser power and fluctuation of laser power due to laser beam deformation.

Attenuation consists of absorption and scattering of the laser light photons by the different aerosols and gaseous molecules in the atmosphere. Laser beam deformation occurs because of small-scale dynamic changes in the index of refraction of the atmosphere. This causes laser beam wander, laser beam spreading, and distortion of the wavefront or scintillation [7].

3.1. Atmospheric Attenuation

3.1.1 Absorption

A selective absorption of radiations that propagate at specific optical wavelength in the atmosphere results from the interaction between photons and atoms or molecules (N_2 , O_2 , H_2 , H_2O , CO_2 , O_3 , Ar, etc..) which leads to the disappearing of the incident photon and an elevation of the temperature. The absorption coefficient depends on the type of gas molecules and on their concentration. Molecular absorption is a selective phenomenon which results in a spectral transmission of the atmosphere presenting transparent zones, called atmospheric transmission window, and opaque zones, called atmospheric blocking windows.

Aerosols are extremely fine solids or liquids particles suspended in the atmosphere with very low fall speed by gravity (ice, dust, smoke, etc). Their size generally lies between 10^{-2} and $100 \mu m$. Fog, dust and maritime spindrift particles are examples of aerosols. Aerosols influence the conditions of atmospheric attenuation due to their chemical nature, their size and their concentration [8].

3.1.2 Scattering

In addition to absorption losses, scattering losses contribute to attenuation of the energy, as a result of elastic collisions of light waves with atmospheric particles. As the beam propagates, the path losses are integrated along the line of sight until the laser light reaches the receiver. The scattering losses occur from all sizes of particles relative to the laser wavelength.

Rayleigh scattering behavior refers to molecular and dust particles that are much smaller than the wavelength of the laser transmission. The angular scattering distribution is dependent upon the polarization of the laser. The scattering loss decreases with longer wavelengths and is only important at lower, UV and visible wavelengths.

Mie scattering, the lower visibility conditions, due to haze, rain, snow, and fog events are responsible for limiting free space optical ranges. The elastic scattering is due to all particles (assumed spherical) that are comparable to the laser wavelength, and is responsible for dominant atmospheric propagation losses. Haze scattering is caused by particles a few microns in size and falls off as the wavelength increases. However, significant scattering attenuations occur only when the rain and snow rates increase or there is increase in fog densities [9].

3.2. Atmospheric Fluctuation

Occasional burst errors of the order of 1 ms or less occur during laser communication transmission primarily due to small-scale dynamic variations in the index of refraction of the atmosphere. Atmospheric turbulence (i.e., wind) produces temporary pockets of air with slightly different temperatures, different densities, and thus different indices of refraction. These air pockets are continuously being created and then destroyed as they are mixed. Data can be lost due to beam wander and scintillation as the laser beam becomes deformed propagating through these index of refraction in-homogeneities. The significance of each effect depends on the size of these turbulence cells with respect to the laser beam diameter. If the size of the turbulence cells is larger than the beam diameter, the laser beam as a whole randomly bends, causing possible signal loss if the beam wanders off the receiver aperture (see Fig. 3.1). More commonly, if the size of the turbulence cells is smaller than the laser beam diameter, ray bending and diffraction cause distortions in the laser beam wavefront. Small variations in the arrival time of various components of the beam wavefront produce constructive and destructive interference, and result in temporal fluctuations in the laser beam intensity at the receiver. These fluctuations in receive power are similar to the twinkling of a distant star. The constant mixing of the atmosphere produces unpredictable turbulent cells of all sizes, resulting in received signal strength fluctuations that are a combination of beam wander and scintillation. Scintillation fluctuations occur on a time scale comparable to the time it takes these cells to move across the beam path due to the wind (see Figure 3.2). Scintillation

fluctuations can be reduced by using either multiple transmit beams or large receiver apertures [7].

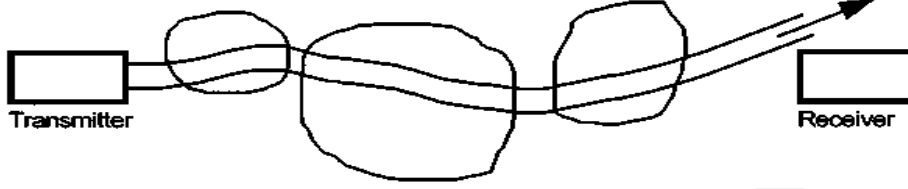


Figure 3.1: Laser beam wander due to turbulence cells which are larger than the beam diameter.

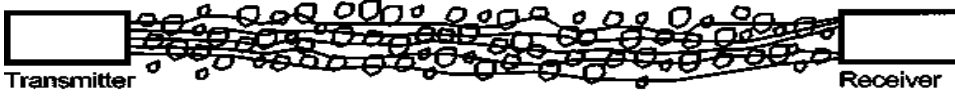


Figure 3.2: Scintillation or fluctuations in beam intensity at the receiver due to turbulent cells that are smaller than the beam diameter.

3.3 The Extended Huygens-Fresnel Principle

The fundamental problem of optical wave propagation was the determination of the field at an observation point, given a disturbance specified over some finite aperture.

In the laser beam propagation, we define $u(\mathbf{s}, 0) = u(s_x, s_y, 0)$ and $u(\mathbf{p}, L) = u(p_x, p_y, L)$ as the input and output fields of a linear system. In the atmosphere, the field changes with the distance L . The field at the receiver can be expressed as

$$u(p_x, p_y, L) = G(\mathbf{s}, \mathbf{p}; L) \otimes u(s_x, s_y, 0), \quad (3.1)$$

where \otimes is the convolution operator and $G(\mathbf{s}, \mathbf{p}; L)$ is the Green's function defined as

$$G(\mathbf{s}, \mathbf{p}; L) = \frac{1}{4\pi L} \exp\left[ikL + \frac{ik}{2L} |\mathbf{s} - \mathbf{p}|^2 \right] \exp[\psi(\mathbf{s}, \mathbf{p})]. \quad (3.2)$$

Here $\psi(\mathbf{s}, \mathbf{p})$ is the random part of the complex phase of a spherical wave propagating in the turbulent medium from the point $(\mathbf{s}, 0)$ to the point (\mathbf{p}, L) .

If $u(\mathbf{p}, L)$ denotes the optical wave field at the transmitter, the field of the wave after propagating a distance L through a random medium is defined by the extended Huygens-Fresnel principle defined as [10]

$$u(\mathbf{p}, L) = -2ik \int_{-\infty}^{\infty} \int_{-\infty}^{\infty} G(\mathbf{s}, \mathbf{p}; L) u(\mathbf{s}, 0) d^2\mathbf{s}, \quad (3.3)$$

$$u(\mathbf{p}, L) = \frac{k}{2i\pi L} \exp(ikL) \int_{-\infty}^{\infty} \int_{-\infty}^{\infty} u(\mathbf{s}, 0) \exp\left[\frac{ik}{2L} |\mathbf{s} - \mathbf{p}|^2 \right] \exp[\psi(\mathbf{s}, \mathbf{p})] d^2\mathbf{s}. \quad (3.4)$$

Using Eq. (3.4) we can find the intensity from $u(\mathbf{p}, L)u^*(\mathbf{p}, L)$, * denoting the complex conjugate.

CHAPTER 4

GENERATING DIFFERENT BEAM'S SOURCE EQUATION FROM GENERAL SOURCE BEAM FORMULA

In this section the existing optical beam fields such as Bessel, Bessel Gaussian, Laguerre, Laguerre Gaussian, Dark Hollow, Bottle, Super Gaussian, Lorentz and Flat-topped beams are combined in a single general source beam formulation.

Source equation of different beams can be generated from the general source beam formula. General source beam wave at the source plane ($z=0$, z being the propagation axis) will have an electric field distribution of

$$\begin{aligned}
 u(s_x, s_y, 0) = & \sum_{l=1}^N A_l T_l \frac{\left[P(s_x^2 + s_y^2)^{\gamma_1} + R(s_x^2 + s_y^2)^{\gamma_2} \right]^{\gamma_3}}{\left(d_1 \alpha_{sxl}^2 + d_3 s_x^2 \right)^{c_1} \left(d_2 \alpha_{syl}^2 + d_4 s_y^2 \right)^{c_2}} \\
 & * (A - V) \exp \left[-j (V_{xl} s_x + V_{yl} s_y) \right] \\
 & * H_n(a_{xl} s_x + b_{xl}) H_m(a_{yl} s_y + b_{yl}), \tag{4.1}
 \end{aligned}$$

where s_x and s_y are the x and y components of the source plane vector \mathbf{s} , i.e., $\mathbf{s} = (s_x, s_y)$. All ℓ subscripted terms establish the specific parameters of the individual beams comprising the general beam through summation. In this manner, N denotes the number of beams, A_ℓ is the complex amplitude of the field at the origin of the source plane, $H_n(a_{x\ell} s_x + b_{x\ell})$ and $H_m(a_{y\ell} s_y + b_{y\ell})$ are Hermite polynomials governing the beam variations for s_x and s_y directions, where n and

m are the order, $a_{x\ell}$ and $a_{y\ell}$ characterize the width, $b_{x\ell}$ and $b_{y\ell}$ are the complex shift parameters, $V_{x\ell}$, $V_{y\ell}$ are the complex displacement parameters, used to create physical location displacement and phase rotation or a combination of both, $\alpha_{xx\ell}$ and $\alpha_{yy\ell}$ are the source sizes, k is the wave number,

$$V = \left\{ C \exp \left[-D \left(\frac{s_x}{(\alpha_{xx\ell})^{f_1}} \right)^{F_1} - E \left(\frac{s_y}{(\alpha_{yy\ell})^{f_2}} \right)^{F_2} \right] - G \exp \left[-Q \left(\frac{s_x}{(\alpha_{xx\ell})^{f_1}} \right)^{F_4} - W \left(\frac{s_y}{(\alpha_{yy\ell})^{f_2}} \right)^{F_5} - jm_2\phi \right] \right\}^{F_3}, \quad (4.2)$$

ϕ is the phase factor and the other parameters such as T_r , P , R , γ_1 , γ_2 , γ_3 , d_1 , d_2 , d_3 , d_4 , c_1 , c_2 , A , B , C , D , E , G , Q , W , F_1 , F_2 , F_3 , F_4 , F_5 , m_2 , f_1 , f_2 are the variable parameters which change with the beam type which we want to generate.

The intensity of the optical wave is the squared magnitude of the field. Thus, at the source plane, the intensity is

$$I(\mathbf{s}, 0) = |u(\mathbf{s}, 0)|^2 \quad (4.3)$$

where $u(\mathbf{s}, 0) = u(s_x, s_y, 0)$. The intensity distribution of the general beam at the exit plane of the laser can be calculated by using Eq. (4.3) for all the cases.

4.1 Limiting Cases

From the general source beam formulation given by Eq. (4.1), the above mentioned beams' source equations can be obtained in the limiting cases. Also the mentioned beams' intensities can be calculated by using Eq. (4.1) and Eq. (4.3). Here Eq. (4.1) is checked and found to reduce to the following limiting cases correctly.

4.1.1 Bessel Beam

Diffraction is an interesting wonder that is a feature of the wave nature of light. It has the possibility of happening anytime when a beam of light passes through an opening

or aperture that is large with respect to its wavelength. According to the Huygens-Fresnel Principle, every point of the wavefront that is unobstructed by the hindrance serves as a source of spherical wavelets that constructively and destructively interfere with each other depending on their optical path length. This creates what is called a diffraction pattern.

Durnin showed that Bessel functions could be used to create exact solutions to the free space wave equation given by :

$$\left(\nabla^2 - \frac{1}{c^2} \frac{\partial^2}{\partial t^2} \right) E(\mathbf{r}, t) = 0. \quad (4.4)$$

These solutions are surprisingly non-diffracting in their propagation. [11]

The zeroth-order Bessel beam is one such solution and results in a beam with a narrow central region surrounded by a series of concentric rings. For an ideal Bessel beam, the electric field is proportional to the zeroth-order Bessel function J_0 :

$$E(r, \phi, z, t) = E_0 \exp[i(-\omega t + k_{||} z)] J_0(k_{\perp} r) \quad (4.5)$$

where $k_{||} = \frac{2\pi}{\lambda} \cos\theta$ and $k_{\perp} = \frac{2\pi}{\lambda} \sin\theta$. Bessel functions of the first kind is defined as

$$J_n(s_x) = \sum_{\tau=0}^{\infty} \frac{(-1)^{\tau} (s_x/2)^{2\tau+n}}{\tau!(\tau+n)!}, \quad (4.6)$$

where n is the order of Bessel function. Defining the relevant parameters in Eq.(4.5) as $z=0$ and $t=0$ Bessel beam source equation can be obtained as

$$\begin{aligned}
E(r, \phi, 0, 0) &= E_0 \exp \left[i \left(-\omega \cdot 0 + \frac{2\pi}{\lambda} \cos \theta \cdot 0 \right) \right] J_0 \left(\frac{2\pi}{\lambda} \sin \theta r \right) \\
&= J_0 \left(\frac{2\pi}{\lambda} \sin \theta r \right) \\
&= \sum_{\tau=0}^{\infty} \frac{\left(-\frac{\pi^2}{\lambda^2} \sin^2 \theta \right)^{\tau} (s_x^2 + s_y^2)}{\tau! \tau!},
\end{aligned} \tag{4.7}$$

Defining the relevant parameters in Eq. (4.1) as

$$\begin{aligned}
l &= \xi + 1, N \rightarrow \infty, A_l = \frac{E_0 \left(-\frac{\pi^2}{\lambda^2} \sin^2 \theta \right)^{\xi}}{\xi! \Gamma(\xi + 1)}, T_r = 1, P = 1, \\
\gamma_1 &= \xi, R = 0, \gamma_3 = 1, c_1 = 0, c_2 = 0, A = 2, F_3 = 0, \\
n &= 0, m = 0, V_{xl} = 0, V_{yl} = 0,
\end{aligned} \tag{4.8}$$

Bessel beam can be obtained. Substituting the parameter set in Eq. (4.8) into Eq. (4.1) and Eq. (4.2) Bessel beam source equation is obtained [12]. After substitution, the reduced form of the general source beam equation can be written as

$$\begin{aligned}
u(s_x, s_y, 0) &= \sum_{\zeta=0}^{\infty} E_0 (s_x^2 + s_y^2)^{\zeta} \\
&\quad \times \frac{\left(-\frac{\pi^2}{\lambda^2} \sin^2 \theta \right)^{\zeta}}{\zeta! \Gamma(\zeta + 1)},
\end{aligned} \tag{4.9}$$

where E_0 is a constant, λ being the wavelength and $\Gamma(n)$ is the gamma function, where $\Gamma(n) = (n-1)!$.

Substituting Eq. (4.1) and Eq. (4.2) into Eq. (4.3), Bessel beam intensity at the source plane is calculated by using the general source beam formulation. Figure 4.1 shows the Bessel beam intensity at the source plane.

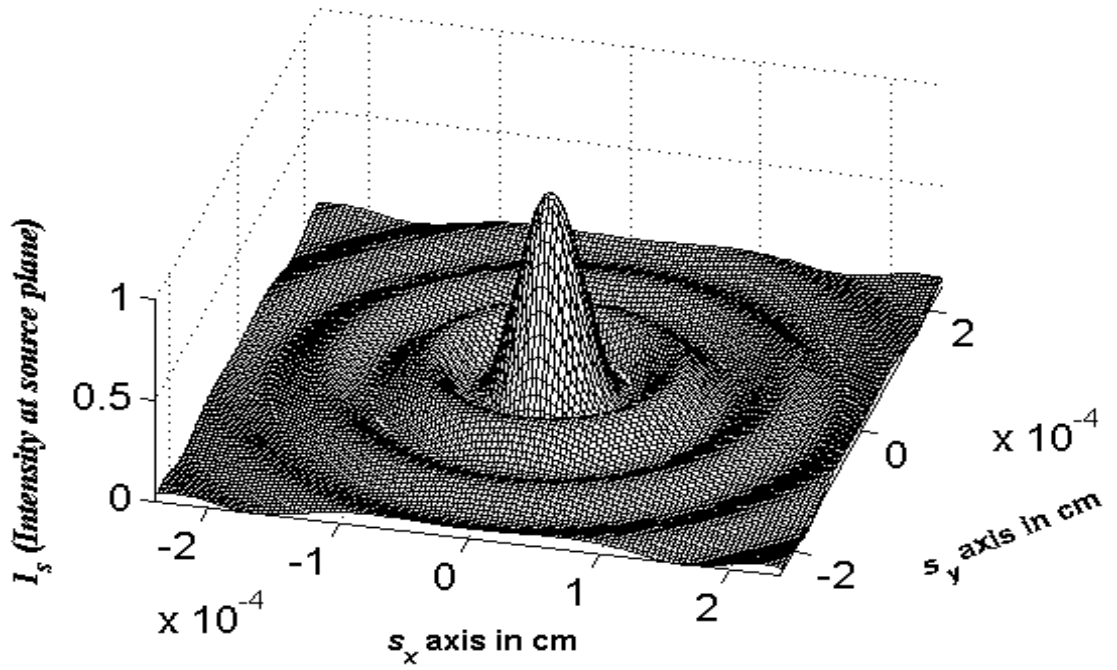


Figure 4.1: Intensity distribution of Bessel beam at the source plane.

4.1.2 Bessel Gaussian Beam

Bessel Gaussian beam is found by multiplying Bessel beam equation by the Gaussian expression which can be defined as

$$u(s_x, s_y, 0) = E_0 \exp\left(-\frac{s_x^2}{2\alpha_{sx}^2} - \frac{s_y^2}{2\alpha_{sy}^2}\right), \quad (4.10)$$

where E_0 is a constant that represents the amplitude. Multiplying Eq. (4.9) by Eq. (4.10), Bessel Gaussian source equation can be obtained. Defining the relevant parameters in Eq. (4.1) as

$$l = \xi + 1, N \rightarrow \infty, A_l = \frac{E_0 \left(-\frac{\pi^2}{\lambda^2} \sin^2 \theta\right)^\xi}{\xi! \Gamma(\xi + 1)}, T_r = 1, P = 1, \gamma_1 = \xi,$$

$$R = 0, \gamma_3 = 1, c_1 = 0, c_2 = 0, A = 0, B = 0, C = 1, D = \frac{1}{2}, F_1 = 2,$$

$$E = \frac{1}{2}, F_2 = 2, G = 0, F_3 = 1, n = 0, m = 0, V_{xl} = 0,$$

$$V_{yl} = 0, f_1 = 1, f_2 = 1,$$

(4.11)

Bessel Gaussian beam is obtained. Substituting Eq. (4.11) into Eq. (4.1) and Eq. (4.2) the general source beam formula reduces to the Bessel Gaussian source equation as

$$u(s_x, s_y, 0) = \sum_{\zeta=0}^{\infty} E_0 (s_x^2 + s_y^2)^{\zeta} \frac{\left(-\frac{\pi^2}{\lambda^2} \sin^2 \theta\right)^{\zeta}}{\zeta! \Gamma(\zeta + 1)} \times \exp\left(-\frac{s_x^2}{2\alpha_{sx}^2} - \frac{s_y^2}{2\alpha_{sy}^2}\right), \quad (4.12)$$

which is a Bessel Gaussian source equation. This correctly checks with reference[13]

4.1.3 Laguerre Beam

The Laguerre beam modes are approximate solutions to the wave equation in cylindrical coordinates, which are valid when the wave propagates in nearly parallel beams. The beam-mode superposition representing the transverse electric field E of an axially-symmetric beam, in cylindrical polar coordinates (r, ϕ, z) , with the z-axis being coincident with the beam axis, where $r = \sqrt{s_x^2 + s_y^2}$. Laguerre source field equation can be defined as [14]

$$u_{mn}(r, \phi, 0) = \left(\frac{\sqrt{2}r}{W_0}\right) L_n^m\left(\frac{2r^2}{W_0^2}\right) \exp(-jm\phi), \quad (4.13)$$

where $L_n^m(x)$ is the associated Laguerre function which can be described as

$$L_n^m(x) = \sum_{k=0}^n (-1)^k \frac{(n+m)!}{(n-k)!(m+k)!k!} x^k, \quad (4.14)$$

and W_0 is the width of the beam waist. Defining the relevant parameters in Eq. (4.1)

as

$$\ell = \zeta + 1, A_\ell = \frac{(-1)^\zeta (N + m_3)!}{(\alpha_{xxl}^{m_3+2\zeta})(N - \zeta)!(m_3 + \zeta)!\zeta!},$$

$$T_r = 1, P = 1, R = 0, \gamma_1 = \xi + \frac{m_3}{2}, \gamma_3 = 1, F_3 = 1, c_1 = 0, c_2 = 0, A = 0,$$

$$B = 0, C = 0, G = 1, Q = 0, W = 0, m_2 = m_3, V_{xl} = 0,$$

$$V_{yl} = 0, n = 0, m = 0, \quad (4.15)$$

Laguerre beam is obtained. After substituting Eq. (4.15) into Eq. (4.1) and Eq. (4.2), the reduced form of Eq. (4.1) can be written as

$$u_{m_3N}(r, \phi, 0) = \sum_{\zeta=0}^N \frac{(-1)^\zeta (s_x^2 + s_y^2)^{\zeta+m_3/2} (N+m_3)!}{(\alpha_{xxl}^{m_3+2\zeta})(N-\zeta)!(m_3+\zeta)!\zeta!} \times \exp(-jm_3\phi), \quad (4.16)$$

which is a Laguerre source beam equation [14], where N and m_3 are mode numbers of the Laguerre polynomial.

4.1.4 Laguerre Gaussian Beam

Multiplying Eq. (4.16) by the Gaussian expression, Laguerre Gaussian source beam equation is obtained. Defining the relevant parameters in Eq. (4.1) as

$$\ell = \zeta + 1, A_\ell = \frac{(-1)^\zeta (N + m_3)!}{(\alpha_{xxl}^{m_3+2\zeta})(N - \zeta)!(m_3 + \zeta)!\zeta!},$$

$$T_r = 1, P = 1, R = 0, \gamma_1 = \xi + \frac{m_3}{2}, \gamma_3 = 1, c_1 = 0, c_2 = 0, A = 0, \quad (4.17)$$

$$B = 0, C = 0, G = 1, Q = 0.5, W = 0.5, m_2 = m_3, F_3 = 1, F_4 = 2, F_5 = 2$$

$$V_{xl} = 0, V_{yl} = 0, n = 0, m = 0,$$

Laguerre Gaussian beam is obtained. After substituting Eq. (4.17) into Eq. (4.1) and Eq. (4.2), the general source beam formulation reduces to

$$\begin{aligned}
u_{m_3 N}(r, \phi, 0) = & \sum_{\zeta=0}^N \frac{(-1)^\zeta (s_x^2 + s_y^2)^{\zeta+m_3/2} (N+m_3)!}{(\alpha_{sxl}^{m_3+2\zeta})(N-\zeta)!(m_3+\zeta)!\zeta!} \\
& \times \exp\left(-\frac{s_x^2}{2\alpha_{sxl}^2} - \frac{s_y^2}{2\alpha_{syl}^2} - jm_3\phi\right),
\end{aligned} \tag{4.18}$$

which is the Lagurre Gaussian source field equation [14]. Also the intensity can be calculated by using Eq. (4.3).

In reference [15] diffractive optics are used to create low and high-order Laguerre-Gaussian beams from the output of a diode laser. They examine the mode purities, conversion efficiencies, extinction ratios, and propagation characteristics. They constructed Laguerre-Gaussian laser beams using diffractive optics in collaboration with the research department of Diffractive Optics Corporation. Using optics they created Laguerre-Gaussian (0,1), Laguerre-Gaussian (1,2), Laguerre-Gaussian (2,3), Laguerre-Gaussian (0,5), and Laguerre-Gaussian (1,10) laser modes. Images of intensity cross sections for these beams are fitting with our intensity distribution profile which we generate by using Eq.(4.1), Eq(4.2) and Eq.(4.3).

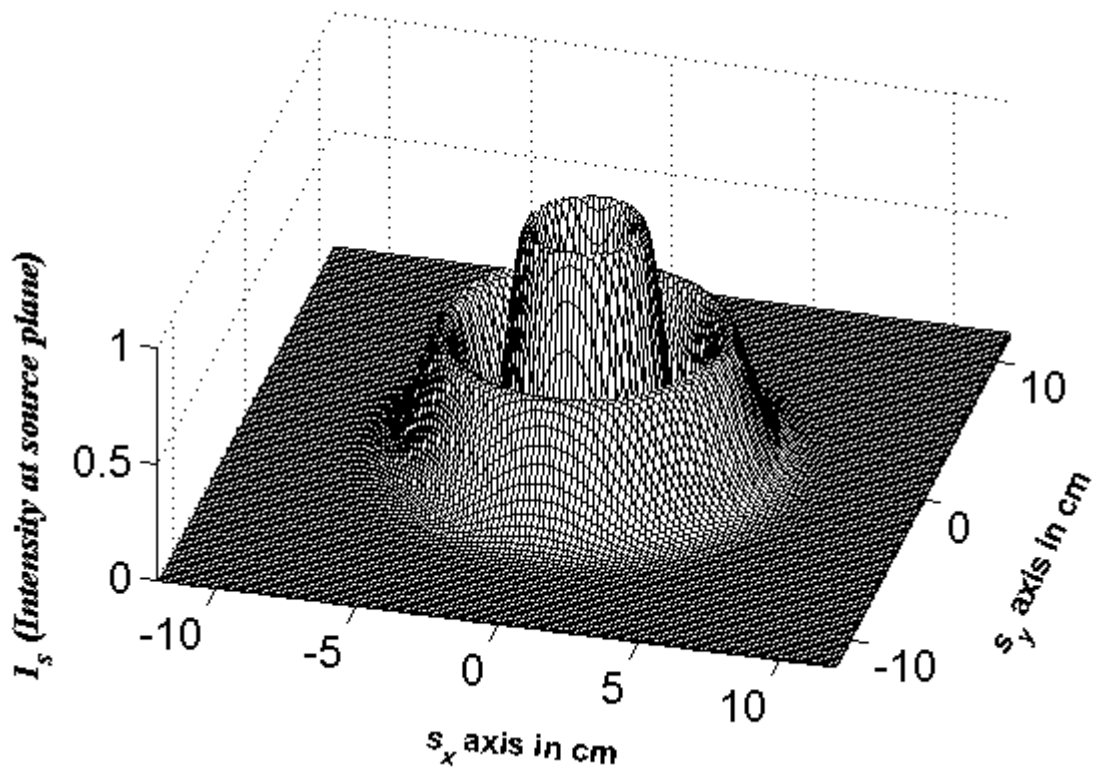


Figure 4.2: Intensity distribution of Laguerre Gaussian beam at the source plane with mode orders (1,2).

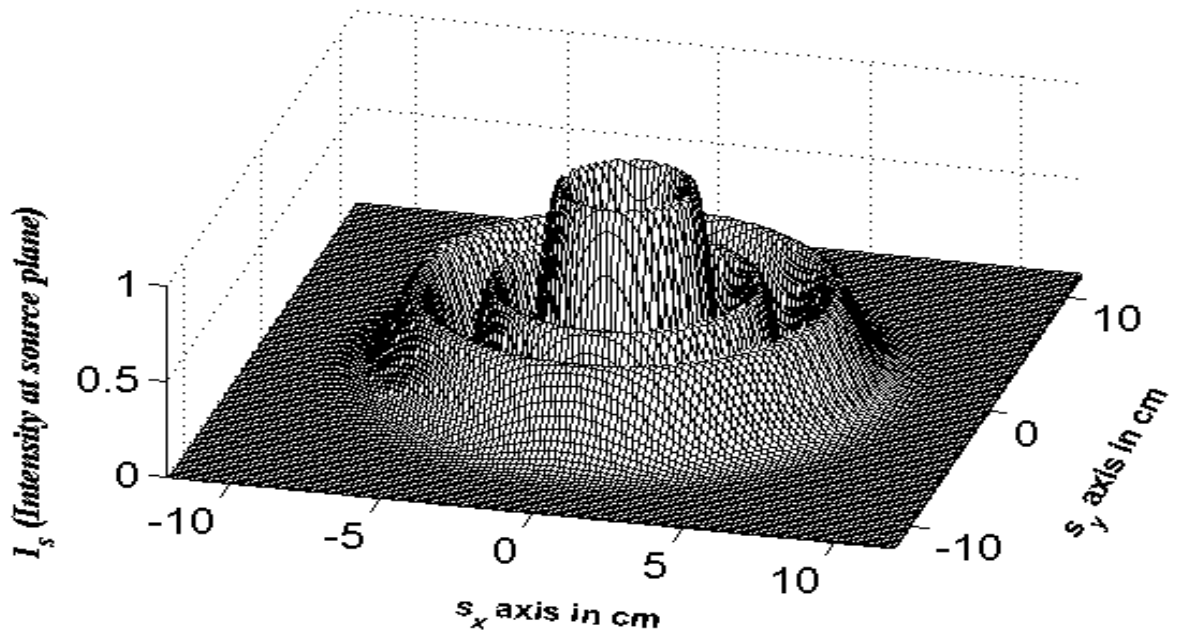


Figure 4.3: Intensity distribution of Laguerre Gaussian beam at the source plane with mode orders (2,3).

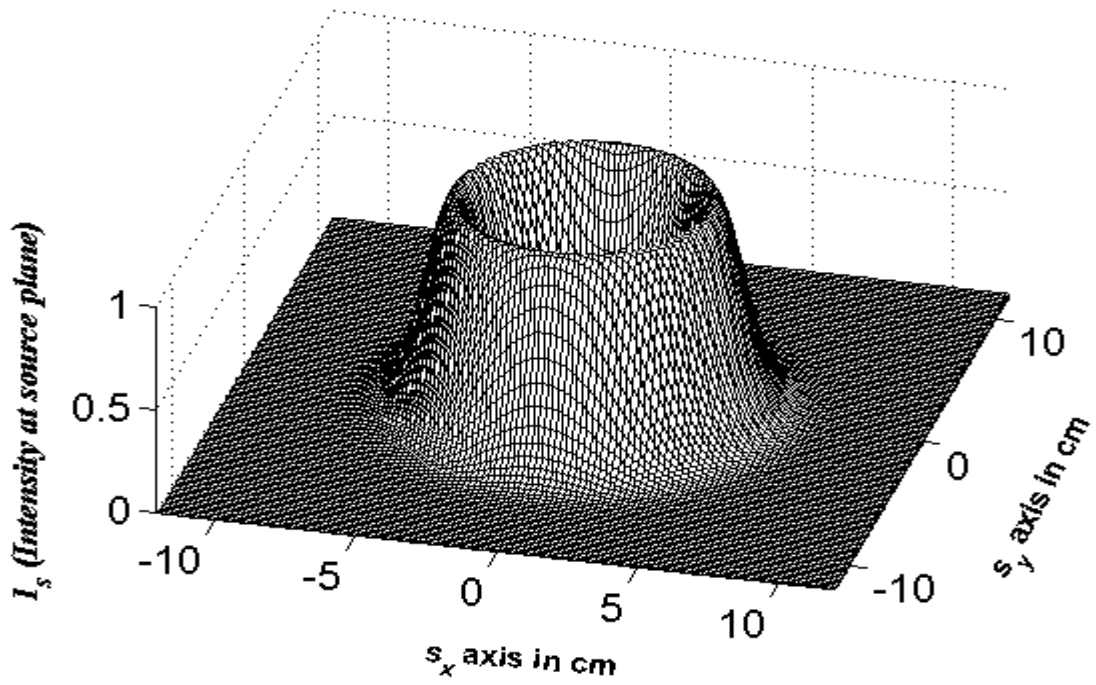


Figure 4.4: Intensity distribution of Laguerre Gaussian beam at the source plane with mode orders (0,5).

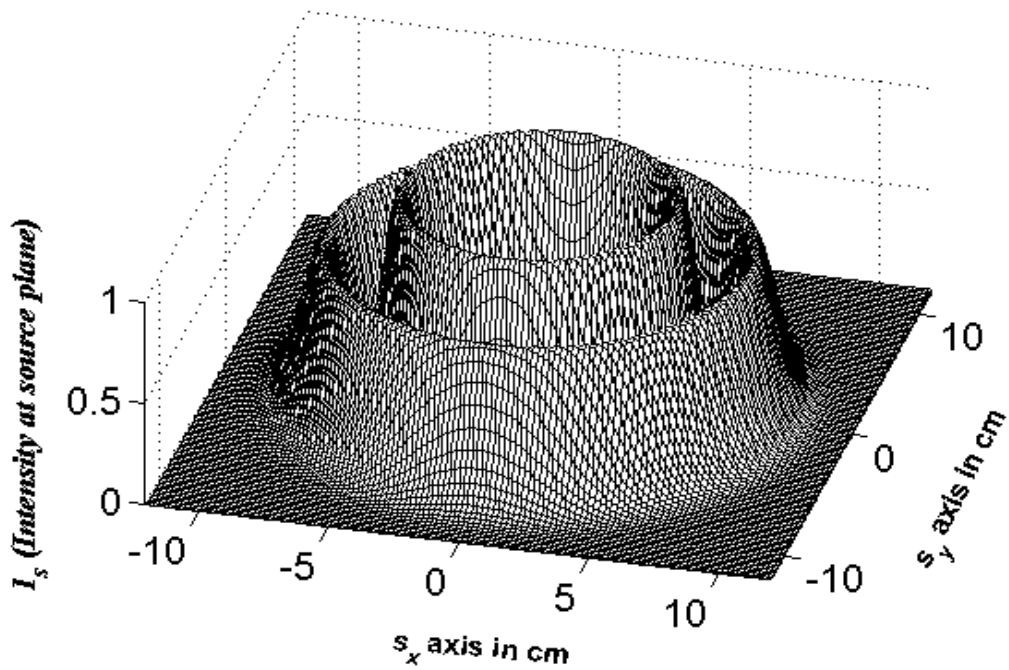


Figure 4.5: Intensity distribution of Laguerre Gaussian beam at the source plane with mode orders (1,10).

4.1.5 Dark Hollow Beam

In recent years, dark-hollow beams (DHBs) have attracted more and more attention because of their wide applications in modern optics and atomic optics. DHBs have been widely studied both experimentally and theoretically. A DHB can be expressed as a finite sum of Laguerre-Gaussian beams or Gaussian beams. [16]

The electric field of a dark hollow beam at $z = 0$ can be expressed as the following finite sum of Gaussian beams

$$u(s_x, s_y, 0) = \sum_{n=1}^N \frac{(-1)^{n-1}}{N} \binom{N}{n} \times \left[\exp\left(-\frac{ns_x^2 + ns_y^2}{W_0^2}\right) - \exp\left(-\frac{ns_x^2 + ns_y^2}{pW_0^2}\right) \right], \quad (4.19)$$

where $\binom{N}{n}$ denotes a binomial coefficient, N is the order of a circular dark hollow beam, W_0 determines the beam waist width, and $p = \varepsilon^2$ with $p < 1$. Defining the relevant parameters in Eq. (4.1) as

$$\begin{aligned} \ell &= \xi, \quad A_\ell = \frac{(-1)^{\xi-1}}{N} \frac{N!}{\xi!(N-\xi)!}, \quad T_r = 1, \quad \gamma_3 = 0, \\ c_1 &= 0, \quad c_2 = 0, \quad A = 0, \quad B = 0, \quad C = 1, \quad D = \frac{\xi}{2}, \quad G = -1, \\ E &= \frac{\xi}{2}, \quad Q = \frac{\xi}{2\varepsilon^2}, \quad F_1 = 2, \quad F_2 = 2, \quad F_3 = 1, \quad F_4 = 2, \quad F_5 = 2 \\ W &= \frac{\xi}{2\varepsilon^2}, \quad m_2 = 0, \quad f_1 = 1, \quad f_2 = 1, \quad V_{x\ell} = 0, \quad V_{y\ell} = 0, \\ n &= 0, \quad m = 0, \end{aligned} \quad (4.20)$$

dark hollow beam is obtained. After substituting Eq. (4.20) into Eq. (4.1) and Eq. (4.2), the general source beam formula reduces to

$$u(s_x, s_y, 0) = \sum_{\zeta=1}^N \frac{(-1)^{\zeta-1}}{N} \frac{N!}{\zeta!(N-\zeta)!} \times \left[\exp\left(-\frac{\zeta s_x^2}{2\alpha_{sxl}^2} - \frac{\zeta s_y^2}{2\alpha_{syl}^2}\right) - \exp\left(-\frac{\zeta s_x^2}{2\varepsilon^2 \alpha_{sxl}^2} - \frac{\zeta s_y^2}{2\varepsilon^2 \alpha_{syl}^2}\right) \right], \quad (4.21)$$

which is dark hollow source beam equation [17]. Using Eq. (4.3) the intensity at source plane can be calculated. Figure 4.6 shows the intensity distribution plot of dark hollow beam at the source plane.

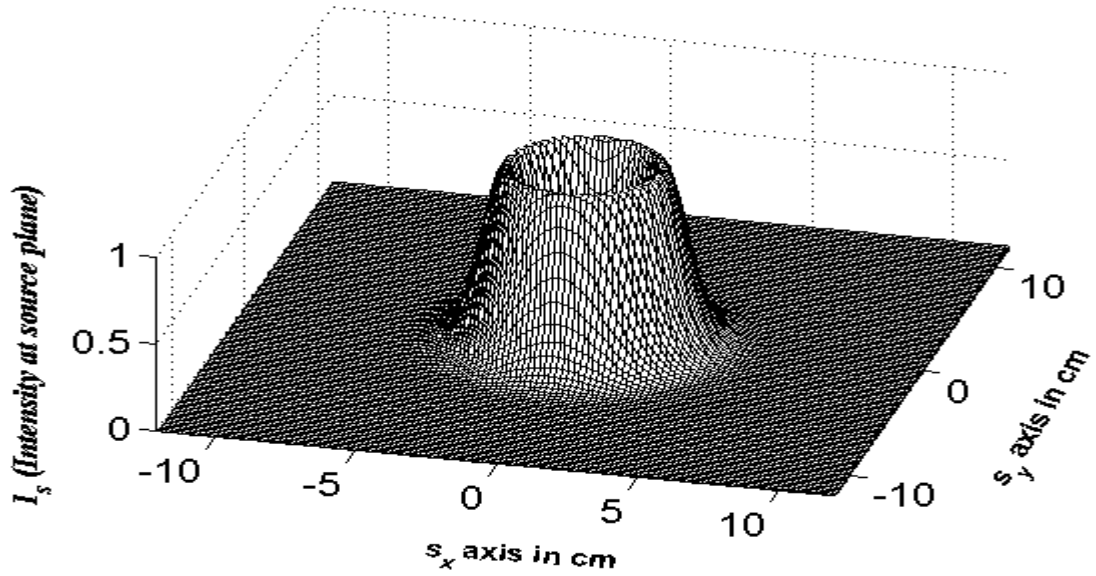


Figure 4.6: Intensity distribution of dark hollow beam at the source plane.

4.1.6 Bottle Beam

The electric field of the bottle beam can be defined as

$$E(r, \phi, 0) = L_{00}(r, 0) - L_{20}(r, 0), \quad (4.22)$$

where L_{00} and L_{20} are the Laguerre polynomials and $L_{00} = L(0, 0)$, $L_{20} = L(2, 0)$.

Defining the relevant parameters in Eq. (4.1) as

$$\begin{aligned}
 N = 1, A_\ell = 1, T_r = 1, c_1 = 0, c_2 = 0, P = \frac{-1}{2\alpha_{sxl}^4}, \gamma_1 = 2, \\
 R = \frac{2}{\alpha_{syt}^2}, \gamma_2 = 1, \gamma_3 = 1, A = 0, B = 0, C = 1, D = \frac{1}{2}, \\
 E = \frac{1}{2}, G = 0, f_1 = 1, f_2 = 1, F_1 = 2, F_2 = 2, F_3 = 1, \\
 V_{xl} = 0, V_{yl} = 0, n = 0, m = 0,
 \end{aligned} \tag{4.23}$$

bottle beam is obtained. Substituting Eq. (4.23) into Eq. (4.1) and Eq. (4.2), reduced form of the general source beam formulation is

$$\begin{aligned}
 E(r, 0) &= L_{00}(r, z) - L_{20}(r, z) \\
 &= \exp\left(-\frac{1}{2}\left(\frac{s_x^2}{\alpha_{sxl}^2} + \frac{s_y^2}{\alpha_{syt}^2}\right)\right) \\
 &\quad \times \left\{ \frac{-(s_x^2 + s_y^2)^2}{2\alpha_{sxl}^4} + \frac{2(s_x^2 + s_y^2)}{\alpha_{syt}^2} \right\},
 \end{aligned} \tag{4.24}$$

which satisfies bottle beam source equation [18]. With general source beam formulation, the intensity can be calculated by using Eq. (4.3). Figure 4.7 shows the intensity distribution at the source plane.

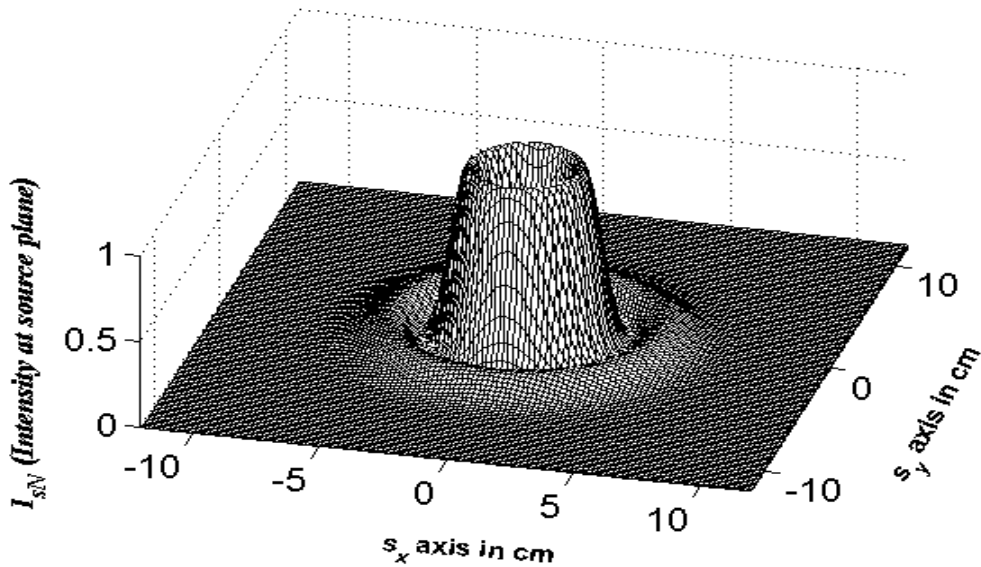


Figure 4.7: Bottle beam intensity at the source plane.

4.1.7 Flat-Topped Beam

Flat-topped (FT) beams are derived from the fundamental Gaussian beam by introducing an order of flatness parameter. They possess a number of attractive features. Amongst these are less spreading in propagation and medical applications.

Flat-topped beam source equation can be defined as

$$u_s(s_x, s_y, 0) = 1 - \left[1 - \exp\left(-s_x^2 / \alpha_{sx}^2 - s_y^2 / \alpha_{sy}^2\right) \right]^{N_f}, \quad (4.25)$$

where N_f is the order parameter for flatness, such that $N_f = 1$. When $N_f \neq 1$, on the other hand, the beam sizes will depart from Gaussian source sizes along s_x and s_y directions. Defining the relevant parameters in Eq. (3.1) as

$$\begin{aligned} N &= 1, A_x = 1, T_r = 1, A = 1, B = 1, C = 1, D = 1, \\ E &= 1, F_1 = 2, F_2 = 2, F_3 = N_f, f_1 = 1, f_2 = 1, \\ G &= 0, V_{xl} = 0, V_{yl} = 0, n = 0, m = 0, \end{aligned} \quad (4.26)$$

flat-topped beam is obtained. Substituting Eq. (4.26) into Eq. (4.1), and Eq. (4.2), the general source beam formulation reduces to a flat-topped beam source equation [19]. The intensity can be calculated using Eq. (4.3). Figure 4.8 is the intensity plot for flat-topped beam at the source plane when $N_f = 8$ and Figure 4.9 is the intensity plot for flat-topped beam at the source plane when $N_f = 5$

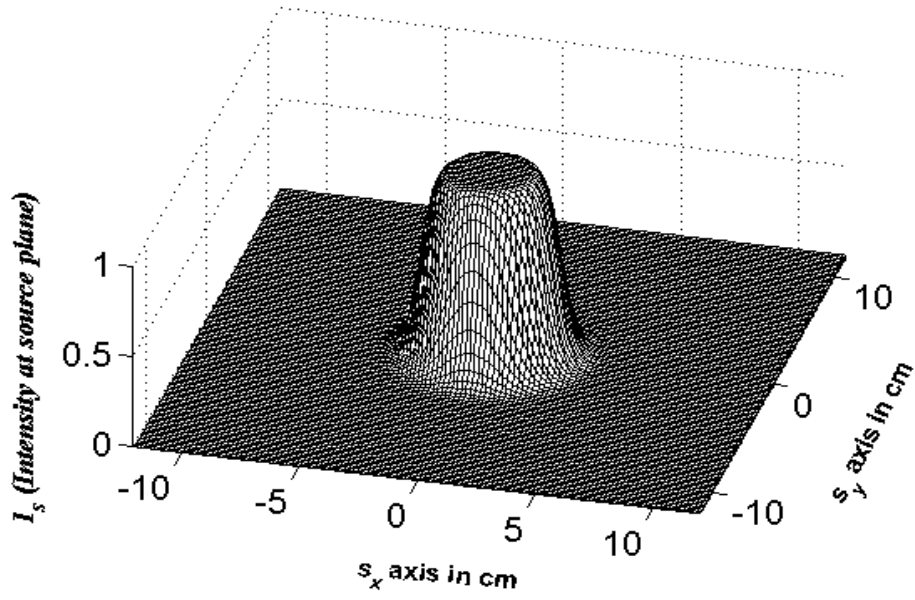


Figure 4.8: Flat-topped intensity at the source plane with $N_f = 8$.

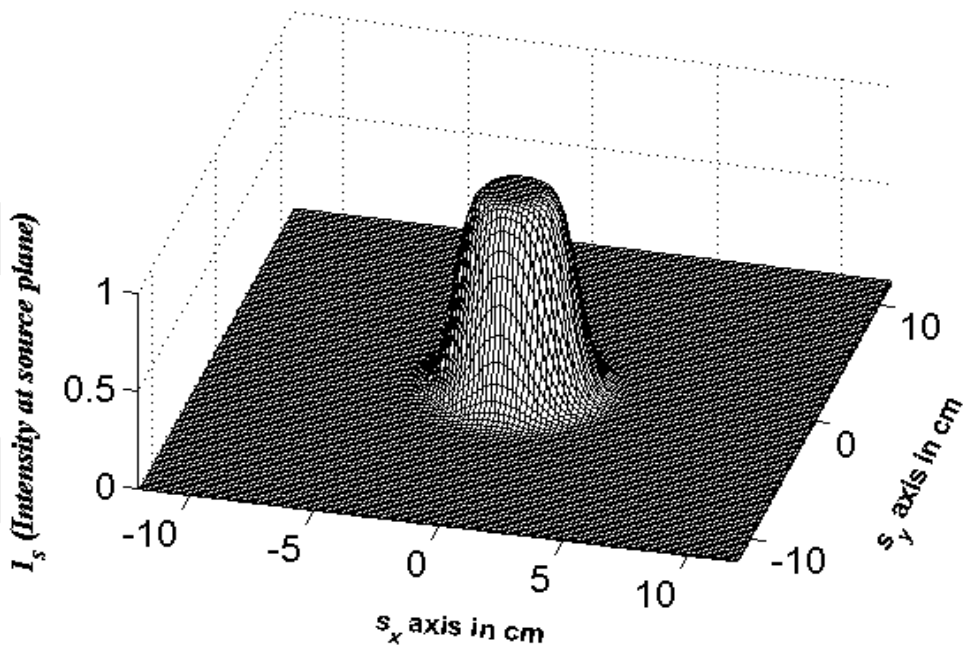


Figure 4.9: Flat-topped intensity at the source plane with $N_f = 5$.

4.1.8 Super Gaussian Beam

Super-Gaussian beam is efficient in extracting laser power in a single lowest order mode with a large user-defined waist, thus improving the beam quality and focusibility. Super Gaussian beam source equation can be defined as

$$u(s_x, s_y, 0) = \exp \left[- \left(\frac{s_x}{\sqrt{2\alpha_{sxl}}} \right)^{N_s} - \left(\frac{s_y}{\sqrt{2\alpha_{syl}}} \right)^{N_s} \right], \quad (4.27)$$

where N_s is the super Gaussian power. [20]

Defining the relevant parameters in Eq. (3.1) as

$$\begin{aligned} N &= 1, T_r = 1, A_\ell = 1, \gamma_3 = 0, c_1 = 0, c_2 = 0, A = 0, B = 0, C = 1, \\ D &= \frac{1}{(\sqrt{2})^{N_s}}, E = \frac{1}{(\sqrt{2})^{N_s}}, G = 0, F_1 = N_s, F_2 = N_s, F_3 = 1, \\ V_{x\ell} &= 0, V_{y\ell} = 0, n = 0, m = 0, f_1 = 1, f_2 = 1, \end{aligned} \quad (4.28)$$

super Gaussian beam is obtained. After substituting Eq. (4.28) into Eq. (4.1) and Eq. (4.2), the general source beam formulation reduces to a super Gaussian beam source equation [20]. Figure 4.10 shows the intensity plot for $N_s = 8$ at the source plane. Figure 4.11 shows the intensity plot for $N_s = 2$ at the source plane.

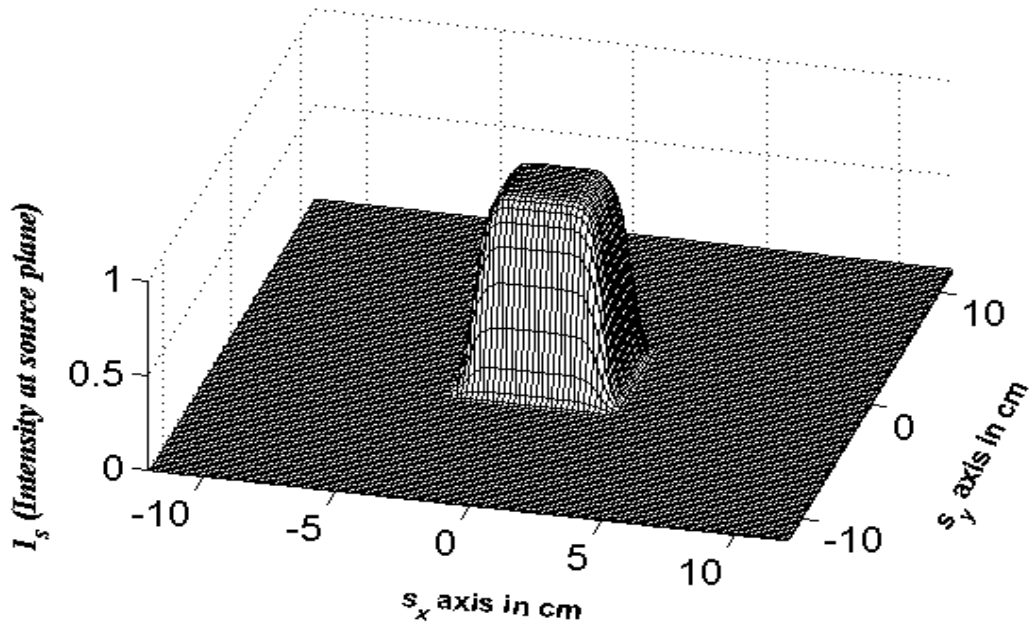


Figure 4.10: Super Gaussian beam intensity at the source plane for $N_s = 8$.

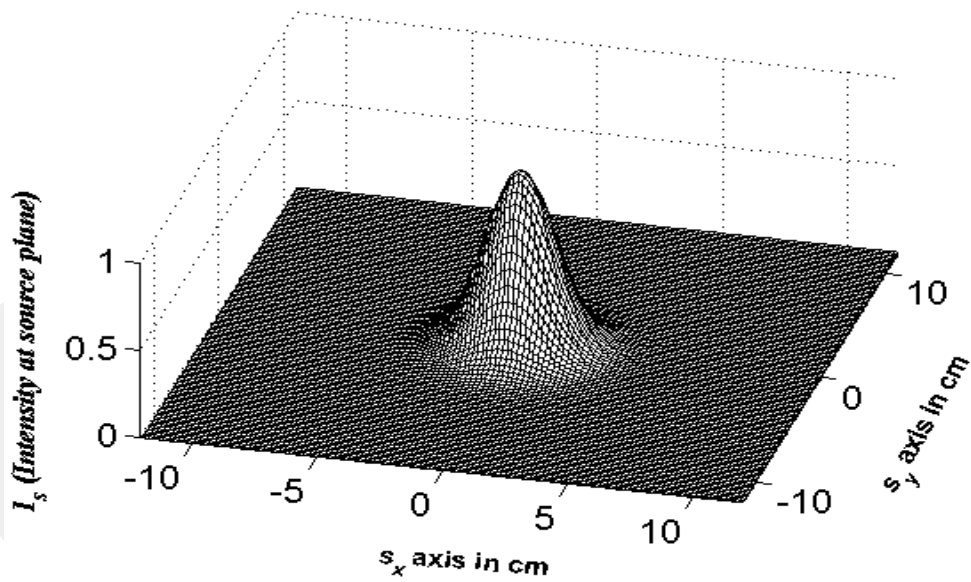


Figure 4.11: Super Gaussian beam intensity at the source plane for $N_s = 2$.

4.1.9 Lorentz Beam

These beams are called Lorentz beams because the form of their transverse pattern in the source plane is the product of two independent Lorentz functions. Lorentz beam source equation can be defined as

$$u(s_x, s_y, 0) = \frac{E_0}{W_x W_y} \frac{1}{\left[1 + (s_x/W_x)^2\right]} \frac{1}{\left[1 + (s_y/W_y)^2\right]}, \quad (4.29)$$

where E_0 is a constant value and W_x and W_y are parameters related to the beam width, $W_x = \sqrt{2}\alpha_{sxl}$ and $W_y = \sqrt{2}\alpha_{syl}$, with A , W_{s_x} and $W_{s_y} \in \mathfrak{R}$. Defining the relevant parameters in Eq. (4.1) as

$$\begin{aligned} N &= 1, A_\ell = 2E_0\alpha_{sxl}\alpha_{syl}, T_r = 1, \gamma_3 = 0, c_1 = 1, c_2 = 1, \\ d_1 &= 2, d_2 = 2, A = 2, F_3 = 0, V_{x\ell} = 0, V_{y\ell} = 0, \\ n &= 0, m = 0, d_3 = 1, d_4 = 1 \end{aligned} \quad (4.30)$$

Lorentz beam is obtained. After substitution of Eq. (4.30) into Eq. (4.1) and Eq. (4.2), the general beam source formulation reduces to

$$u(s_x, s_y, 0) = 2E_0\alpha_{sxl}\alpha_{syl} \frac{1}{(2\alpha_{sxl}^2 + s_x^2)(2\alpha_{syl}^2 + s_y^2)}, \quad (4.31)$$

which is the Lorentz beam source equation [21]. Figure 4.12 shows the intensity plot of Lorentz beam at the source plane.

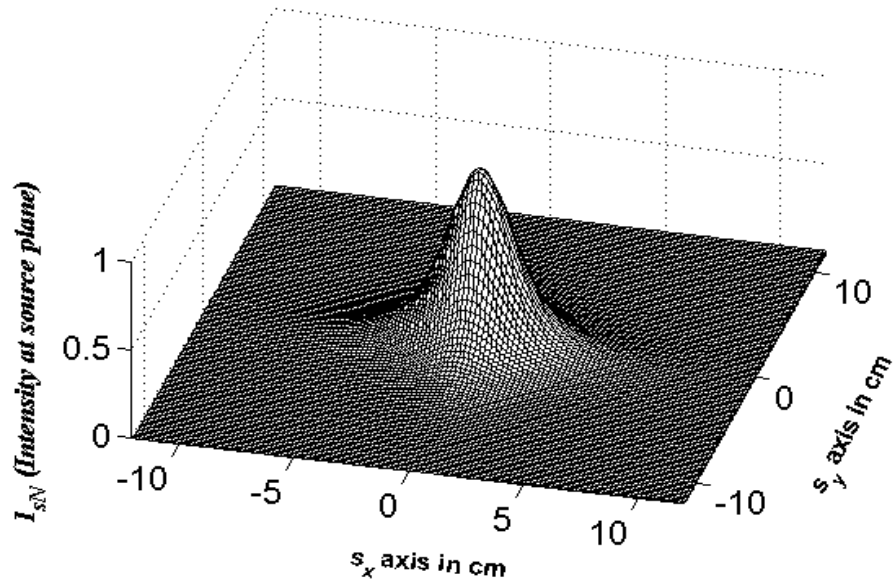


Figure 4.12: Lorentz beam intensity at the source plane.

CHAPTER 5

NUMERICAL CALCULATION OF AVERAGE RECEIVED INTENSITY BY USING GENERAL BEAM FORMULA

In this part, general source beam formulation and Matlab code used to calculate the average received intensity in turbulence, numerically. Here, Eq. (5.1) is used as the source field in the calculation of the average received intensity in turbulence.

$$\begin{aligned}
 u(s_x, s_y, 0) = & \sum_{l=1}^N AT \frac{\left[P(s_x^2 + s_y^2)^{\gamma_1} + R(s_x^2 + s_y^2)^{\gamma_2} \right]^3}{\left(d\alpha_{1\ x}^2 + d s_{3\ x}^2 \right)^{c_1} \left(d\alpha_{2\ y}^2 + d s_{4\ y}^2 \right)^{c_2}} \\
 & *(A-V) \exp[-j(V s_{x\ x} + V s_{y\ y})] \\
 & *H_n(a s_{x\ x} + b) H_m(a s_{y\ y} + b),
 \end{aligned} \tag{5.1}$$

The average intensity $\langle I(\mathbf{p}, L) \rangle$, of the general beam on a receiver plane located at L distance away from the source can be written as

$$\langle I(\mathbf{p}, L) \rangle = \langle u(\mathbf{p}, L) u(\mathbf{p}, L)^* \rangle, \tag{5.2}$$

where

$$u(\mathbf{p}, L) = \frac{k}{2j\pi L} \exp(jkL) \int_{-\infty}^{\infty} \int_{-\infty}^{\infty} d^2s u(\mathbf{s}) \exp\left[jk(\mathbf{p}-\mathbf{s})^2 / 2L + \psi(\mathbf{s}, \mathbf{p}) \right], \tag{5.3}$$

and

$$\begin{aligned}
u(\mathbf{p}, L)u(\mathbf{p}, L)^* &= \frac{k}{2j\pi L} \exp(jkL) \int_{-\infty}^{\infty} \int_{-\infty}^{\infty} \mathbf{d}\mathbf{s}_1^2 u(\mathbf{s}_1) \\
&\quad * \exp\left[jk(\mathbf{p} - \mathbf{s}_1)^2 / 2L + \psi(\mathbf{s}_1, \mathbf{p}) \right] \\
&\quad * \frac{k}{(-2j\pi L)} \exp(-jkL) \int_{-\infty}^{\infty} \int_{-\infty}^{\infty} \mathbf{d}\mathbf{s}_2^2 u^*(\mathbf{s}_2) \\
&\quad * \exp\left[-jk(\mathbf{p} - \mathbf{s}_2)^2 / 2L + \psi^*(\mathbf{s}_2, \mathbf{p}) \right]
\end{aligned} \tag{5.4}$$

After substituting Eq. (5.4) into Eq. (5.2), the average received intensity can be calculated as

$$\begin{aligned}
\langle I(\mathbf{p}, L) \rangle &= \left(\frac{k}{2\pi L} \right)^2 \int_{-\infty}^{\infty} \int_{-\infty}^{\infty} \int_{-\infty}^{\infty} \int_{-\infty}^{\infty} \mathbf{d}\mathbf{s}_1^2 \mathbf{d}\mathbf{s}_2^2 u(\mathbf{s}_1) u^*(\mathbf{s}_2) \\
&\quad * \exp\left\{ jk \left[(\mathbf{p} - \mathbf{s}_1)^2 - (\mathbf{p} - \mathbf{s}_2)^2 \right] / 2L \right\} \\
&\quad * \langle \exp\left[\psi(\mathbf{s}_1, \mathbf{p}) + \psi^*(\mathbf{s}_2, \mathbf{p}) \right] \rangle,
\end{aligned} \tag{5.5}$$

where the ensemble average term within the integrand is

$$\langle \exp\left[\psi(\mathbf{s}_1, \mathbf{p}) + \psi^*(\mathbf{s}_2, \mathbf{p}) \right] \rangle \cong \exp\left[-\rho_0^{-2} (\mathbf{s}_1 - \mathbf{s}_2)^2 \right], \tag{5.6}$$

with ψ being the fluctuations of the complex amplitude, p_x and p_y are the x and y components of the receiver plane vector \mathbf{p} , such that $\mathbf{p} = (p_x, p_y)$, $\rho_0 = (0.545 C_n^2 k^2 L)^{-3/5}$ is the coherence length of a spherical wave propagating in the turbulent medium and C_n^2 is the structure constant. Note that Eq. (5.6) is derived under the quadratic approximation for the Rytov's phase structure function [19], [22] and

$$\begin{aligned}
u(\mathbf{s}_1)u^*(\mathbf{s}_2) = & \sum_{\ell_1=1}^N \sum_{\ell_2=1}^N A_{\ell_1} A_{\ell_2}^* T_r T_r^* \frac{\left[P(s_{x1}^2 + s_{y1}^2)^{\gamma_1} + R(s_{x1}^2 + s_{y1}^2)^{\gamma_2} \right]^{\gamma_3}}{\left(d_1 \alpha_{sx1}^2 + d_3 s_{x1}^2 \right)^{c_1} \left(d_2 \alpha_{sy1}^2 + d_4 s_{y1}^2 \right)^{c_2}} \frac{\left[P(s_{x2}^2 + s_{y2}^2)^{\gamma_1} + R(s_{x2}^2 + s_{y2}^2)^{\gamma_2} \right]^{\gamma_3}}{\left(d_1 \alpha_{sx2}^2 + d_3 s_{x2}^2 \right)^{c_1} \left(d_2 \alpha_{sy2}^2 + d_4 s_{y2}^2 \right)^{c_2}} \\
& * \left[A \left\{ B - C \exp \left[-D \left(\frac{s_{x1}}{\alpha_{sx1}} \right)^{f_1} - E \left(\frac{s_{y1}}{\alpha_{sy1}} \right)^{f_2} \right] - G \exp \left[-Q \left(\frac{s_{x1}}{\alpha_{sx1}} \right)^{f_4} - W \left(\frac{s_{y1}}{\alpha_{sy1}} \right)^{f_5} - jm_2 \phi \right] \right\}^{F_3} \right] \\
& * \left[A \left\{ B - C \exp \left[-D \left(\frac{s_{x2}}{\alpha_{sx2}} \right)^{f_1} - E \left(\frac{s_{y2}}{\alpha_{sy2}} \right)^{f_2} \right] - G \exp \left[-Q \left(\frac{s_{x2}}{\alpha_{sx2}} \right)^{f_4} - W \left(\frac{s_{y2}}{\alpha_{sy2}} \right)^{f_5} - jm_2 \phi \right] \right\}^{F_3} \right] \\
& * \exp \left[-j(V_{x1} s_{x1} + V_{y1} s_{y1}) \right] \exp \left[-j(V_{x2} s_{x2} + V_{y2} s_{y2}) \right] \\
& * H_{m1}(a_{x1} s_{x1} + b_{x1}) H_{m2}(a_{x2} s_{x2} + b_{x2}) H_{m1}(a_{y1} s_{y1} + b_{y1}) H_{m2}(a_{y2} s_{y2} + b_{y2}),
\end{aligned} \tag{5.7}$$

After substituting Eq. (5.7) into Eq. (5.5), the average received intensity can be calculated as

$$\begin{aligned}
\langle I(\mathbf{p}, L) \rangle = & \left(\frac{k}{2\pi L} \right)^2 \int_{-\infty}^{\infty} \int_{-\infty}^{\infty} \int_{-\infty}^{\infty} \int_{-\infty}^{\infty} \mathbf{d}\mathbf{s}_1 \mathbf{d}\mathbf{s}_2 \sum_{\ell_1=1}^N \sum_{\ell_2=1}^N A_{\ell_1} A_{\ell_2}^* T_r T_r^* \langle \exp[\psi(\mathbf{s}_1, \mathbf{p}) + \psi^*(\mathbf{s}_2, \mathbf{p})] \rangle \\
& * \frac{\left[P(s_{x1}^2 + s_{y1}^2)^{\gamma_1} + R(s_{x1}^2 + s_{y1}^2)^{\gamma_2} \right]^{\gamma_3}}{\left(d_1 \alpha_{sx1}^2 + d_3 s_{x1}^2 \right)^{c_1} \left(d_2 \alpha_{sy1}^2 + d_4 s_{y1}^2 \right)^{c_2}} \frac{\left[P(s_{x2}^2 + s_{y2}^2)^{\gamma_1} + R(s_{x2}^2 + s_{y2}^2)^{\gamma_2} \right]^{\gamma_3}}{\left(d_1 \alpha_{sx2}^2 + d_3 s_{x2}^2 \right)^{c_1} \left(d_2 \alpha_{sy2}^2 + d_4 s_{y2}^2 \right)^{c_2}} \\
& * \left[A \left\{ B - C \exp \left[-D \left(\frac{s_{x1}}{\alpha_{sx1}} \right)^{f_1} - E \left(\frac{s_{y1}}{\alpha_{sy1}} \right)^{f_2} \right] - G \exp \left[-Q \left(\frac{s_{x1}}{\alpha_{sx1}} \right)^{f_4} - W \left(\frac{s_{y1}}{\alpha_{sy1}} \right)^{f_5} - jm_2 \phi \right] \right\}^{F_3} \right] \\
& * \left[A \left\{ B - C \exp \left[-D \left(\frac{s_{x2}}{\alpha_{sx2}} \right)^{f_1} - E \left(\frac{s_{y2}}{\alpha_{sy2}} \right)^{f_2} \right] - G \exp \left[-Q \left(\frac{s_{x2}}{\alpha_{sx2}} \right)^{f_4} - W \left(\frac{s_{y2}}{\alpha_{sy2}} \right)^{f_5} - jm_2 \phi \right] \right\}^{F_3} \right] \\
& * \exp \left[-j(V_{x1} s_{x1} + V_{y1} s_{y1}) \right] \exp \left[-j(V_{x2} s_{x2} + V_{y2} s_{y2}) \right] \exp \left\{ jk \left[(\mathbf{p} - \mathbf{s}_1)^2 - (\mathbf{p} - \mathbf{s}_2)^2 \right] / 2L \right\} \\
& * H_{m1}(a_{x1} s_{x1} + b_{x1}) H_{m2}(a_{x2} s_{x2} + b_{x2}) H_{m1}(a_{y1} s_{y1} + b_{y1}) H_{m2}(a_{y2} s_{y2} + b_{y2}),
\end{aligned} \tag{5.8}$$

The intensity is calculated and plotted at the source plane in Chapter 4. In this chapter, the average received intensity of different beams in atmospheric turbulence is calculated by using general source beam formulation Eq.(5.8) and Matlab code numerical calculation.

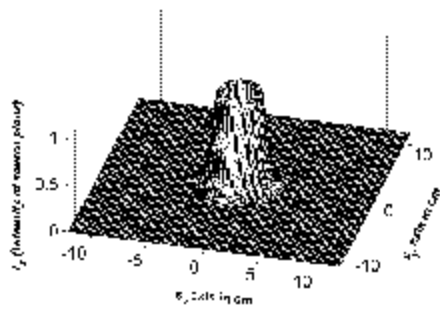
5.1 Dark Hollow Beam

Figure 5.1 shows the normalized average intensity of circular dark hollow beam at several propagation distances in a turbulent atmosphere with $C_n^2=10^{-15} m^{-2/3}$, $w_0=2\text{cm}$, $N=3$, $p=0.9$, $\lambda=632.8\text{nm}$. (the wavelength of a commonly used He-Ne laser). The normalizations in Figure 5.2 and the rest of the figures are carried out with respect to the peak of each beam individually.

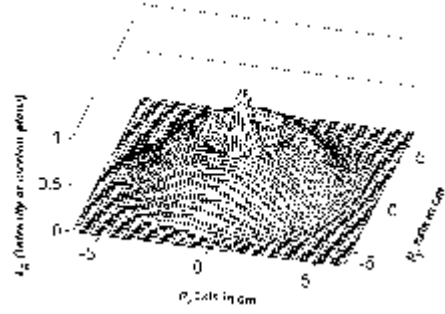
Figure 5.2 shows the normalized average intensity of circular dark hollow beam at several propagation distances in a turbulent atmosphere with $C_n^2=10^{-14} m^{-2/3}$, $w_0=2\text{cm}$, $N=3$, $p=0.9$, $\lambda=632.8\text{nm}$. One can see from Figure 5.2 that the dark hollow beam profile disappears gradually (and the central intensity increases) as propagation distance L increases. While in the far field, the circular DHB becomes a circular Gaussian beam (without a central hollow) in a turbulent atmosphere.

Furthermore, from Figure 5.2, one can also see that the conversion from a circular DHB to a circular Gaussian beam becomes quicker and the beam spot in the far field spreads more rapidly for a larger structure constant.

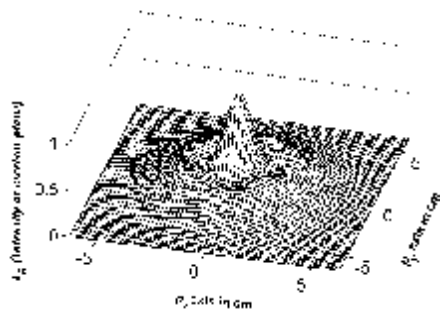
The normalized average intensity of circular dark hollow beam plots matches with reference [16].



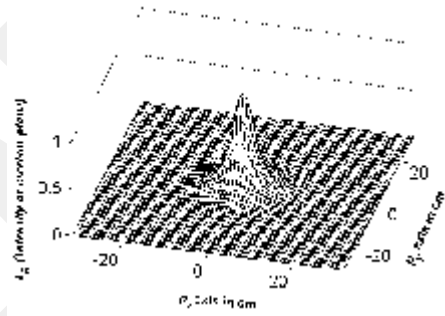
L=0 km



L=1.1 km



L=1.5 km



L=5 km

Figure 5.1: The normalized average intensity of circular dark hollow beam at several propagation distances in a turbulent atmosphere with $C_n^2=10^{-15} m^{-2/3}$, $w_o=2cm$, $N=3$, $p=0.9$, $\lambda=632.8nm$.

disappears gradually as the propagation distance increases, and the flat-topped beam becomes a circular Gaussian beam in the far field.

Furthermore, from Figure 5.4, one can also see that the conversion from a circular flat-topped beam to a circular Gaussian beam becomes quicker and the beam spot in the far field spreads more rapidly for a larger structure constant.

The normalized average intensity of circular flat-topped beam plots matches with reference [23].

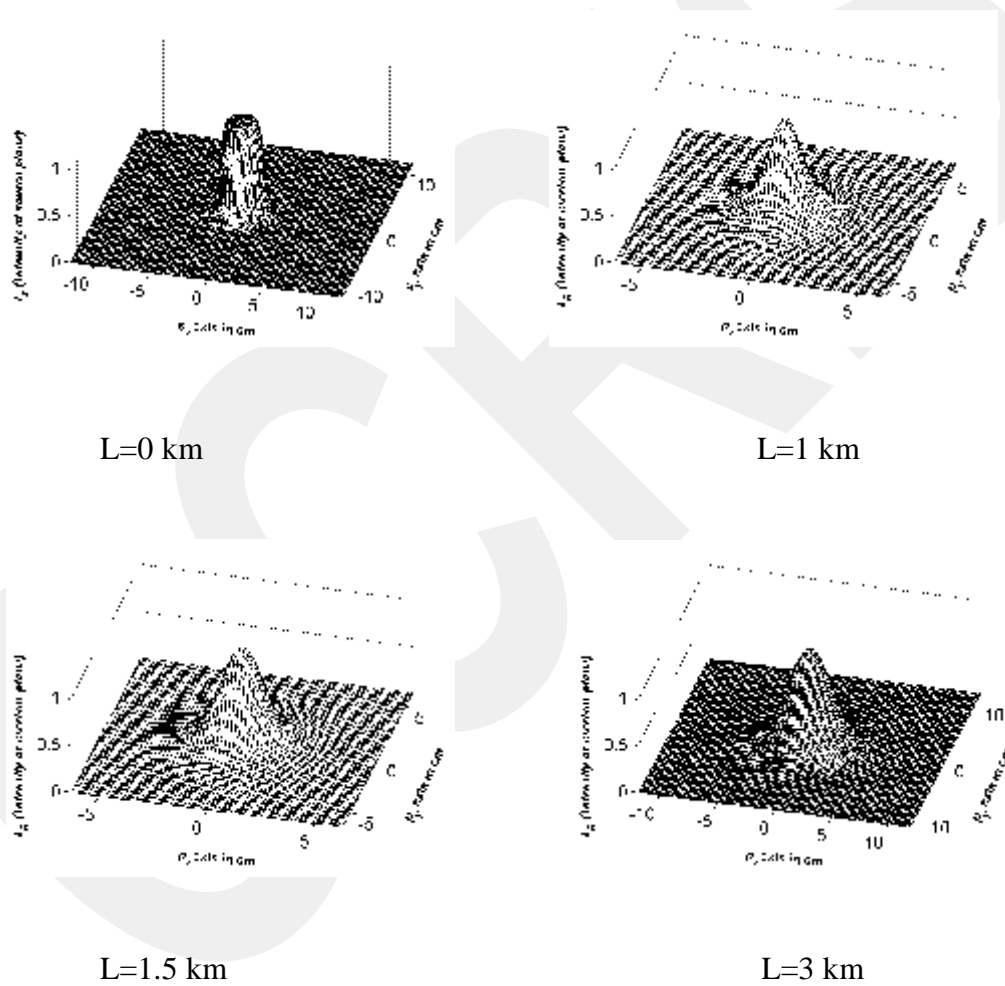


Figure 5.3: The normalized average intensity of circular flat-topped beam at several propagation distances in a turbulent atmosphere with $C_n^2=10^{-15} m^{-2/3}$, $w_o=2cm$, $N_f=8$, $\lambda=632.8nm$.

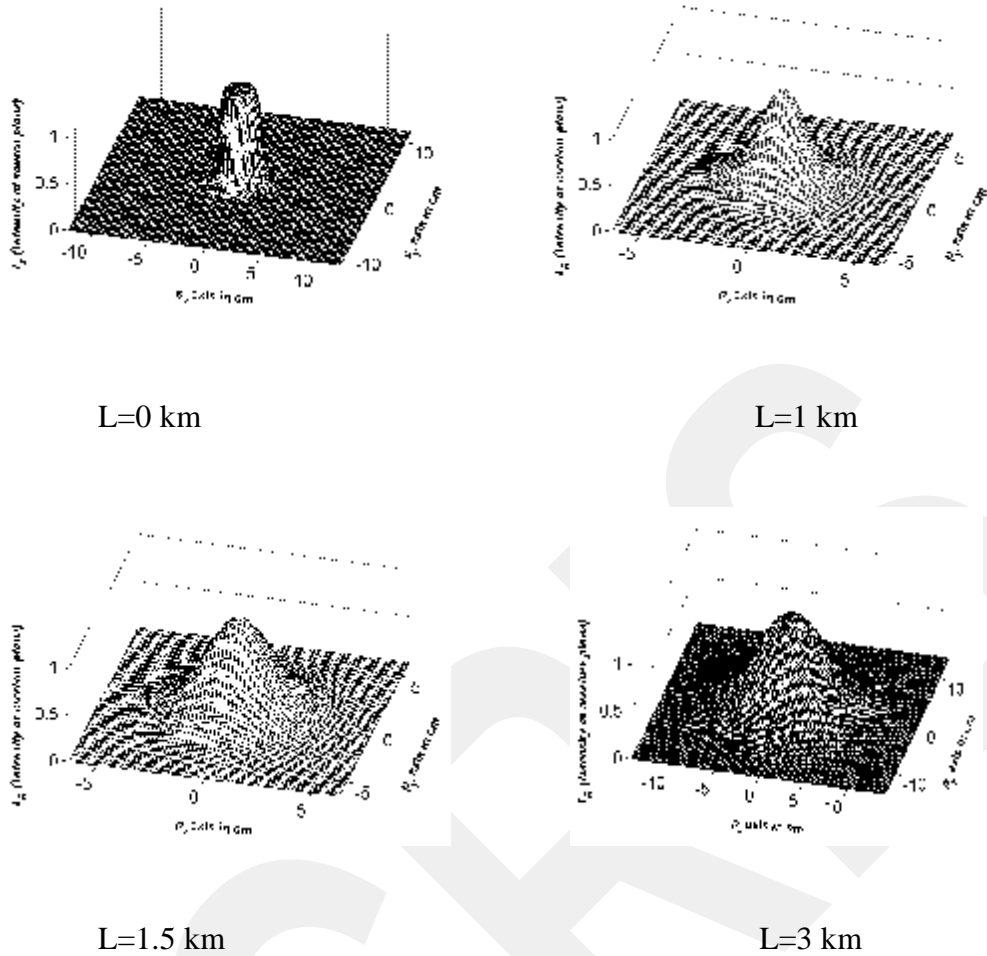


Figure 5.4: The normalized average intensity of circular flat-topped beam at several propagation distances in a turbulent atmosphere with $C_n^2=10^{-14} m^{-2/3}$, $w_o=2cm$, $N_f=8$, $\lambda=632.8nm$.

5.3 Bottle Beam

Figure 5.5 shows the normalized average intensity of bottle beam at several propagation distances in a turbulent atmosphere with $C_n^2=10^{-15} m^{-2/3}$, $w_o=2cm$, $\lambda=632.8nm$.

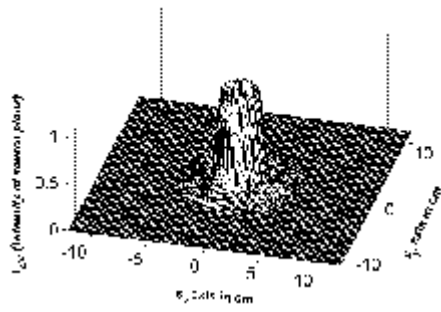
Figure 5.6 shows the normalized average intensity of bottle beam at several propagation distances in a turbulent atmosphere with $C_n^2=10^{-14} m^{-2/3}$, $w_o=2cm$, $\lambda=632.8nm$. In turbulent atmosphere the beam profile disappears gradually as the

propagation distance increases, and the bottle beam becomes a circular Gaussian beam in the far field.

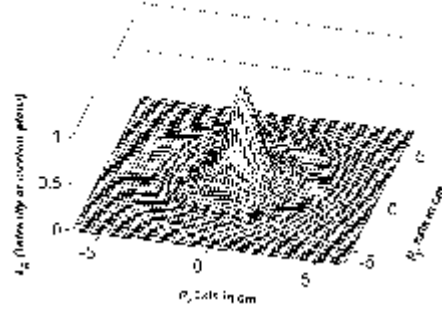
Furthermore, from Figure 5.6, one can also see that the conversion from a bottle beam to a circular Gaussian beam becomes quicker and the beam spot in the far field spreads more rapidly for a larger structure constant.

Figure 5.7 shows the normalized average intensity of bottle beam at several propagation distances in a turbulent atmosphere with $C_n^2=10^{-14}m^{-2/3}$, $w_o=2\text{cm}$, $\lambda=1.55\mu\text{m}$. The beam spot in the far field range spreads more rapidly for longer wavelength.

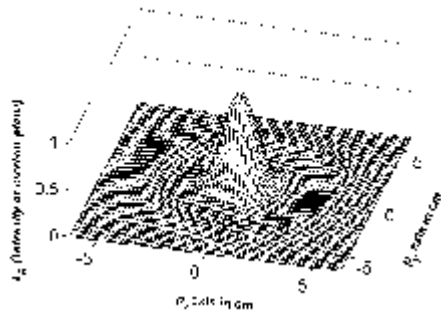
Figure 5.8 shows the normalized average intensity of bottle beam at several propagation distances in a turbulent atmosphere with $C_n^2=10^{-14}m^{-2/3}$, $w_o=4\text{cm}$, $\lambda=632.8\text{nm}$.



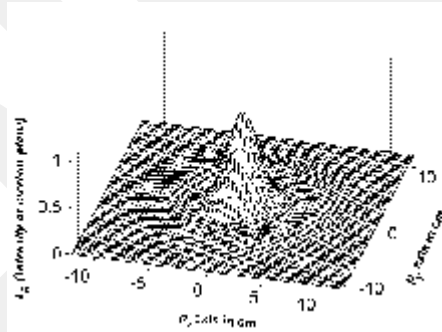
L=0 km



L=1.1 km

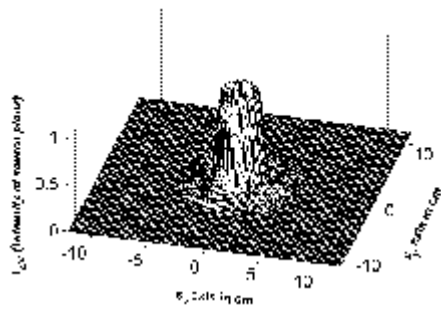


L=1.5 km

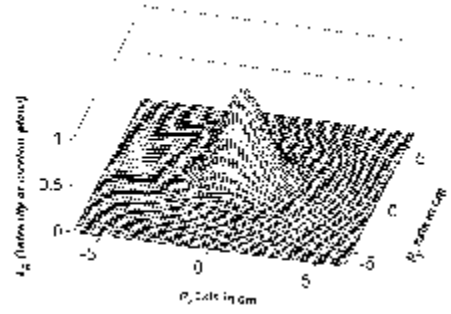


L=3 km

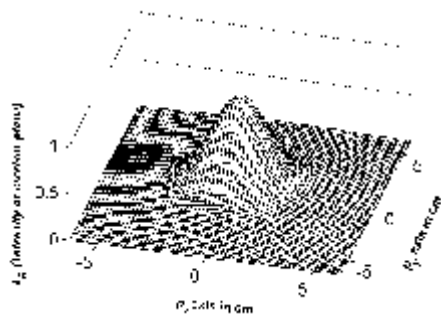
Figure 5.5: The normalized average intensity of bottle beam at several propagation distances in a turbulent atmosphere with $C_n^2=10^{-15} m^{-2/3}$, $w_0=2\text{cm}$, $\lambda=632.8\text{nm}$.



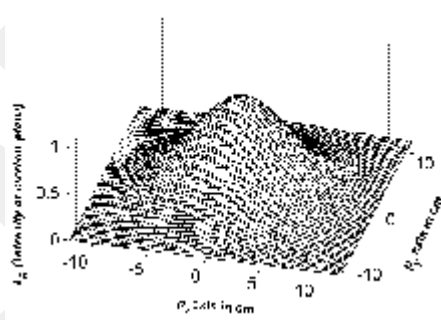
L=0 km



L=1.1 km

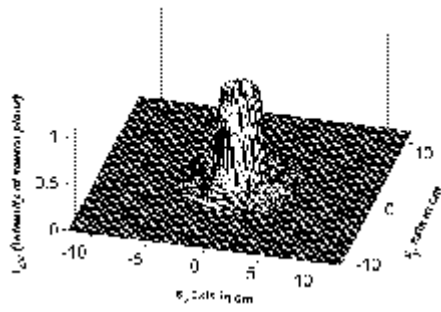


L=1.5 km

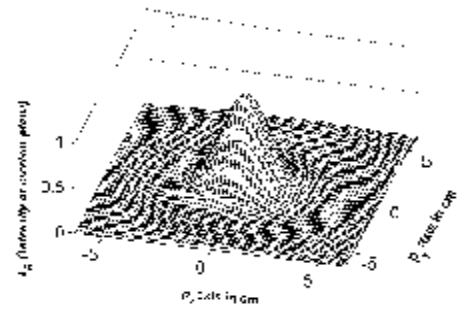


L=3 km

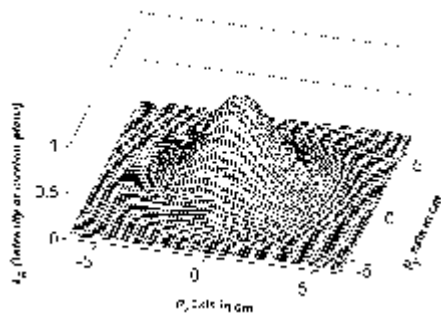
Figure 5.6: The normalized average intensity of bottle beam at several propagation distances in a turbulent atmosphere with $C_n^2=10^{-14}m^{-2/3}$, $w_o=2cm$, $\lambda=632.8nm$.



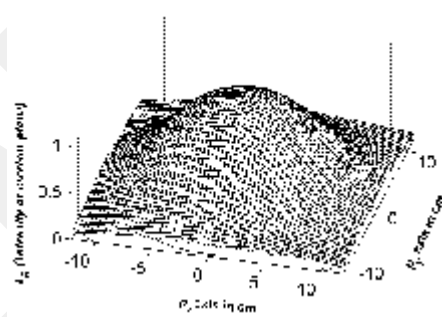
L=0 km



L=1.1 km

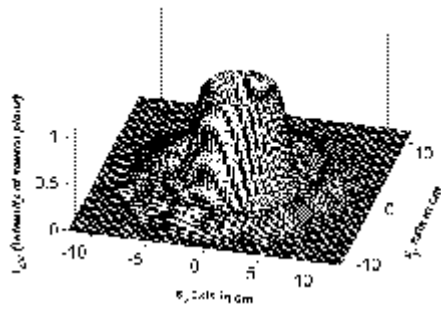


L=1.5 km

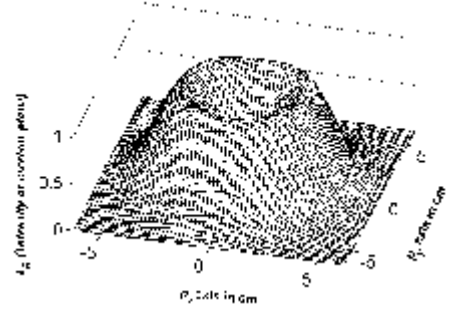


L=3 km

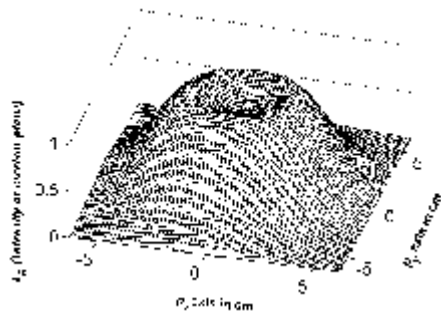
Figure 5.7: The normalized average intensity of bottle beam at several propagation distances in a turbulent atmosphere with $C_n^2=10^{-14} m^{-2/3}$, $w_o=2cm$, $\lambda=1.55 \mu m$.



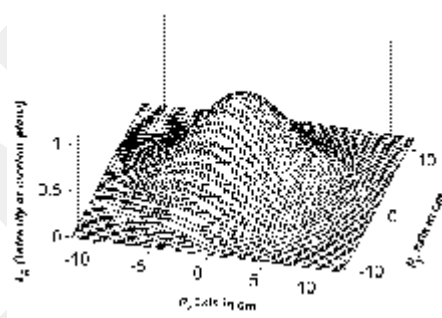
L=0 km



L=1.1 km



L=1.5 km



L=3 km

Figure 5.8: The normalized average intensity of bottle beam at several propagation distances in a turbulent atmosphere with $C_n^2=10^{-14} m^{-2/3}$, $w_o=4cm$, $\lambda=632.8nm$.

5.4 Lorentz Beam

Figure 5.9 shows the normalized average intensity of Lorentz beam at several propagation distances in a turbulent atmosphere with $C_n^2=10^{-15} m^{-2/3}$, $w_o=2\text{cm}$, $\lambda=632.8\text{nm}$.

Figure 5.10 shows the normalized average intensity of Lorentz beam at several propagation distances in a turbulent atmosphere with $C_n^2=10^{-14} m^{-2/3}$, $w_o=2\text{cm}$, $\lambda=632.8\text{nm}$. In turbulent atmosphere the beam profile disappears gradually as the propagation distance increases, and the Lorentz beam becomes a circular Gaussian beam in the far field.

Furthermore, from Figure 5.10, one can also see that the conversion from a Lorentz beam to a circular Gaussian beam becomes quicker and the beam spot in the far field spreads more rapidly for a larger structure constant.

Figure 5.11 shows the normalized average intensity of Lorentz beam at several propagation distances in a turbulent atmosphere with $C_n^2=10^{-14} m^{-2/3}$, $w_o=2\text{cm}$, $\lambda=1.55 \mu\text{m}$. The beam spot in the far field range spreads more rapidly for longer wavelength.

Figure 5.12 shows the normalized average intensity of Lorentz beam at several propagation distances in a turbulent atmosphere with $C_n^2=10^{-14} m^{-2/3}$, $w_o=4\text{cm}$, $\lambda=632.8\text{nm}$.

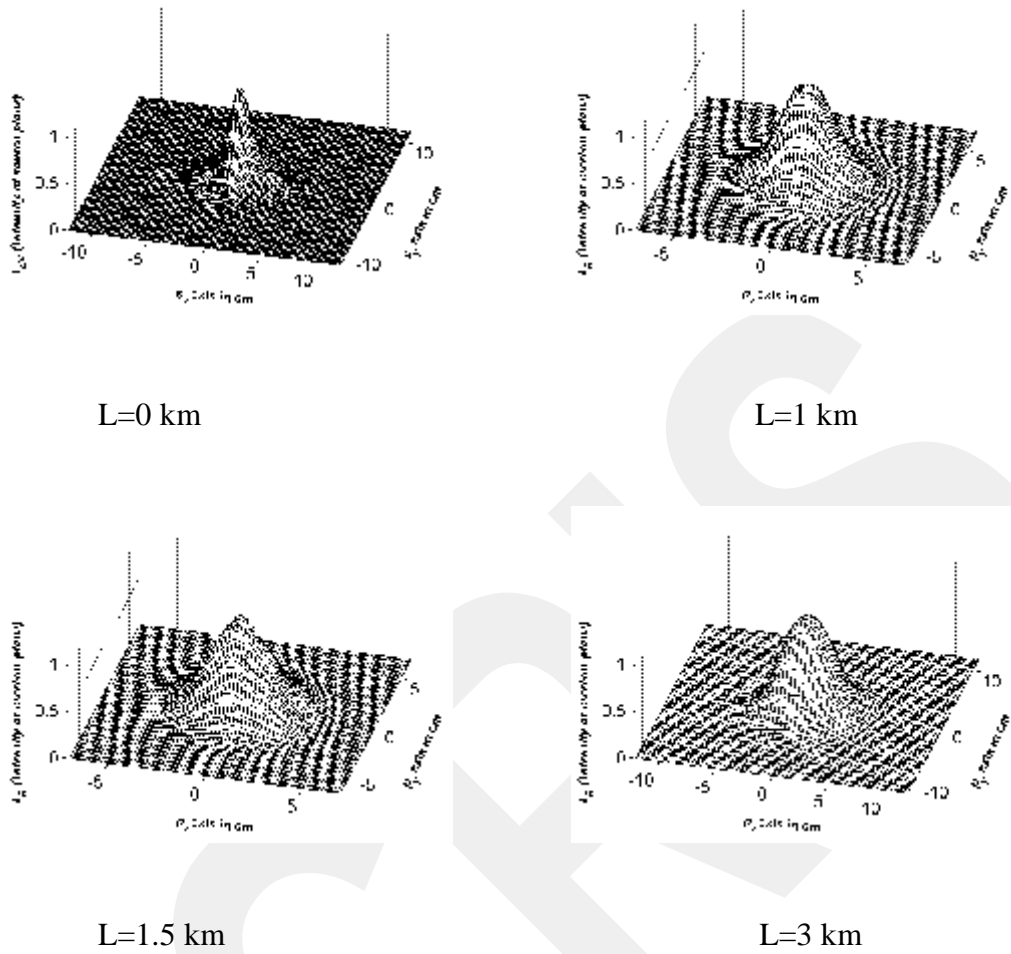
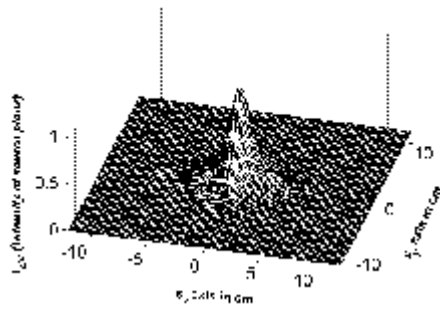
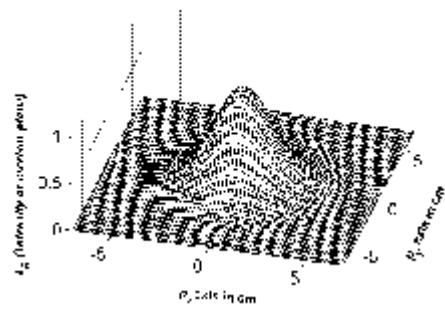


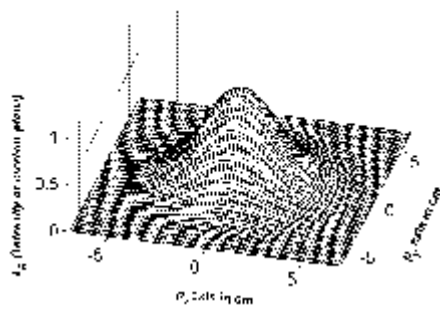
Figure 5.9: The normalized average intensity of Lorentz beam at several propagation distances in a turbulent atmosphere with $C_n^2=10^{-15} \text{m}^{-2/3}$, $w_0=2\text{cm}$, $\lambda=632.8\text{nm}$.



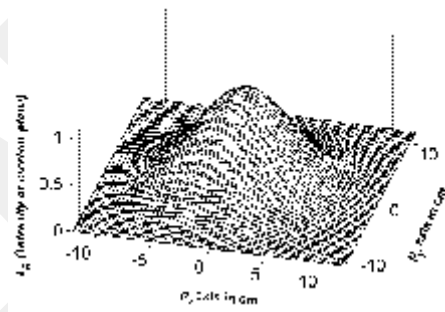
L=0 km



L=1 km

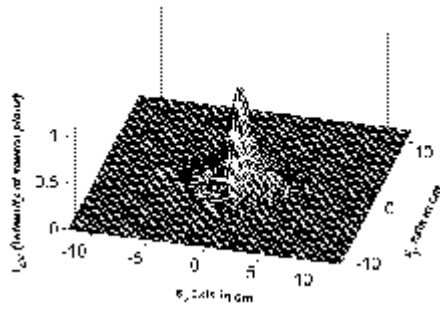


L=1.5 km

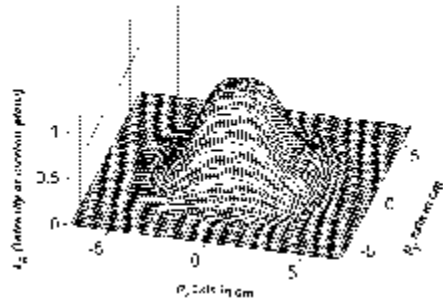


L=3 km

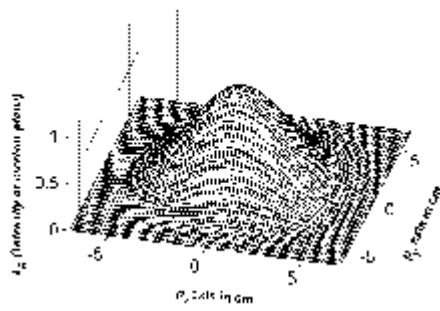
Figure 5.10: The normalized average intensity of lorentz beam at several propagation distances in a turbulent atmosphere with $C_n^2=10^{-14} m^{-2/3}$, $w_o=2cm$, $\lambda=632.8nm$.



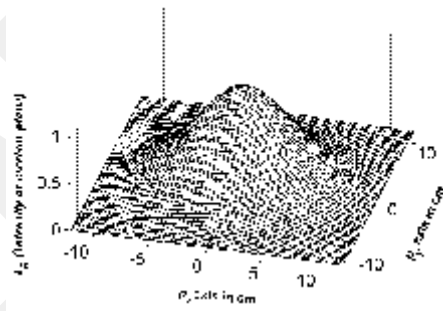
L=0 km



L=1 km



L=1.5 km



L=3 km

Figure 5.11: The normalized average intensity of lorentz beam at several propagation distances in a turbulent atmosphere with $C_n^2=10^{-14} m^{-2/3}$, $w_o=2cm$, $\lambda=1.55 \mu m$.

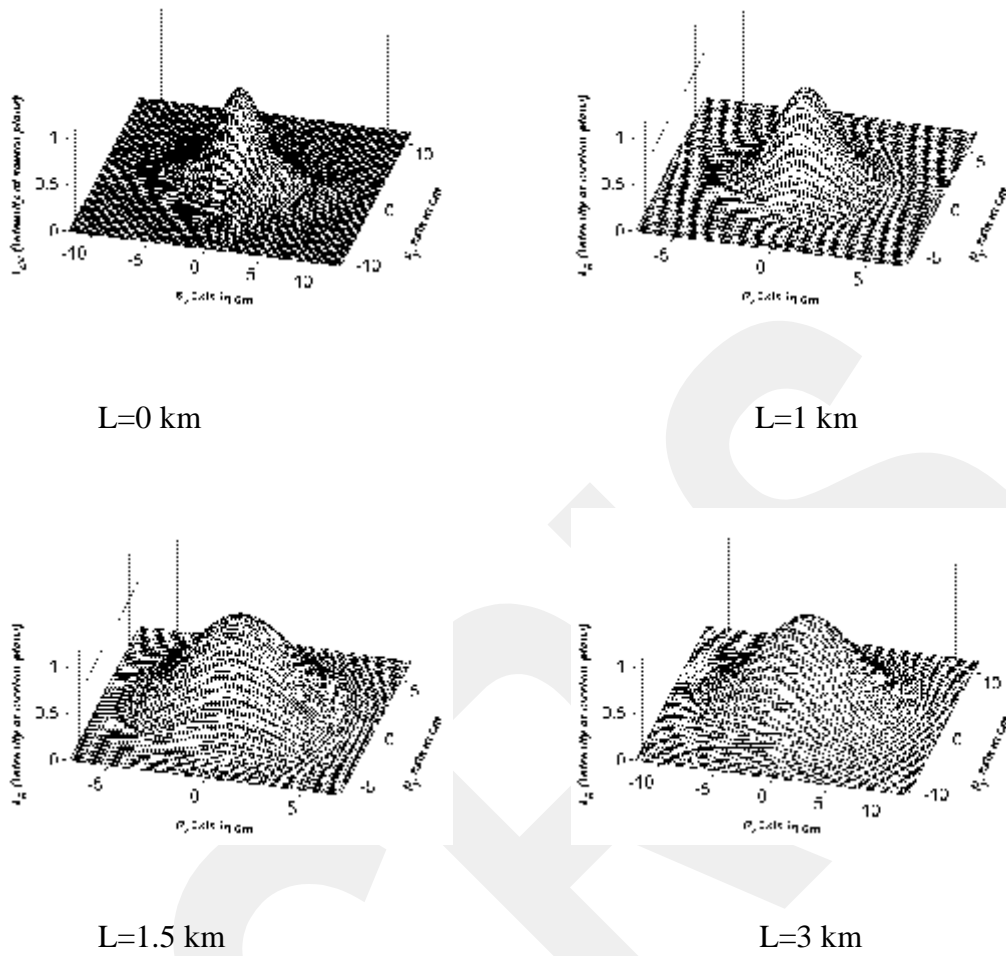


Figure 5.12: The normalized average intensity of Lorentz beam at several propagation distances in a turbulent atmosphere with $C_n^2=10^{-14} m^{-2/3}$, $w_0=4\text{cm}$, $\lambda=632.8\text{nm}$.

5.5 Super Gaussian Beam

Figure 5.13 shows the normalized average intensity of super Gaussian beam at several propagation distances in a turbulent atmosphere with $C_n^2=10^{-15} m^{-2/3}$, $w_0=2\text{cm}$, $\lambda=632.8\text{nm}$.

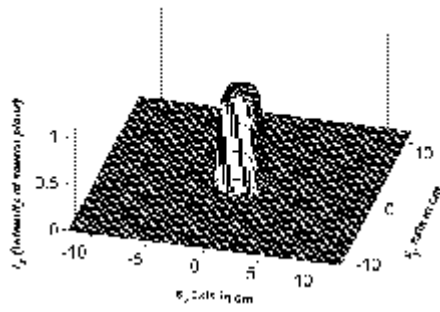
Figure 5.14 shows the normalized average intensity of Super Gaussian beam at several propagation distances in a turbulent atmosphere with $C_n^2=10^{-14} m^{-2/3}$,

$w_o=2\text{cm}$, $\lambda=632.8\text{nm}$. In turbulent atmosphere the beam profile disappears gradually as the propagation distance increases, and the Super Gaussian beam becomes a circular Gaussian beam in the far field.

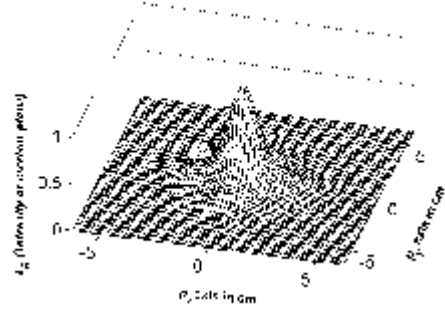
Furthermore, from Figure 5.14, one can also see that the conversion from a Super Gaussian beam to a circular Gaussian beam becomes quicker and the beam spot in the far field spreads more rapidly for a larger structure constant.

Figure 5.15 shows the normalized average intensity of Super Gaussian beam at several propagation distances in a turbulent atmosphere with $C_n^2=10^{-14}\text{m}^{-2/3}$, $w_o=2\text{cm}$, $\lambda=1.55\ \mu\text{m}$. The beam spot in the far field range spreads more rapidly for longer wavelength.

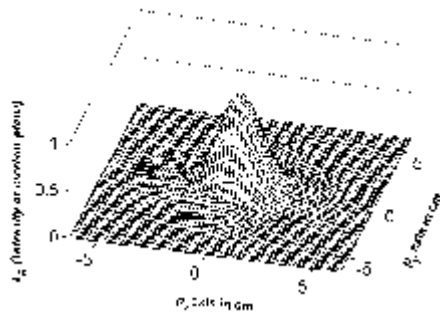
Figure 5.16 shows the normalized average intensity of Super Gaussian beam at several propagation distances in a turbulent atmosphere with $C_n^2=10^{-14}\text{m}^{-2/3}$, $w_o=4\text{cm}$, $\lambda=632.8\text{nm}$.



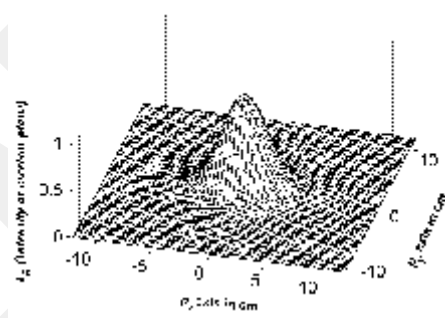
L=0 km



L=1 km

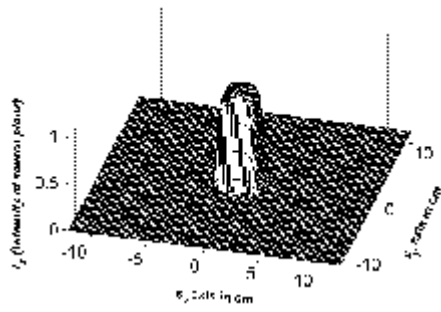


L=1.5 km

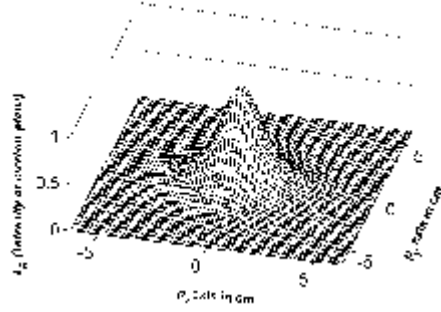


L=3 km

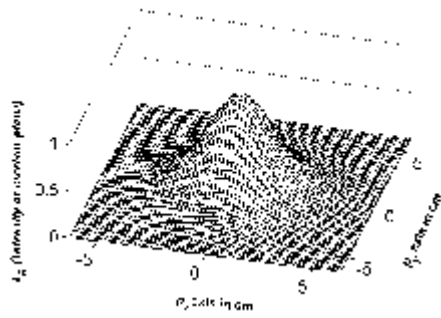
Figure 5.13: The normalized average intensity of Super gaussian beam at several propagation distances in a turbulent atmosphere with $C_n^2=10^{-15} m^{-2/3}$, $w_o=2cm$, $\lambda=632.8nm$.



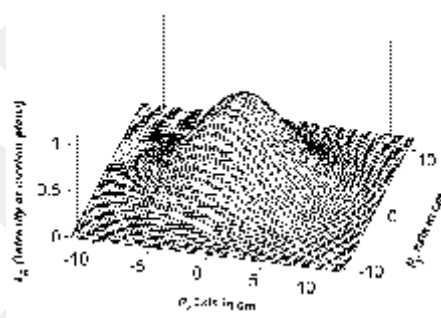
L=0 km



L=1 km

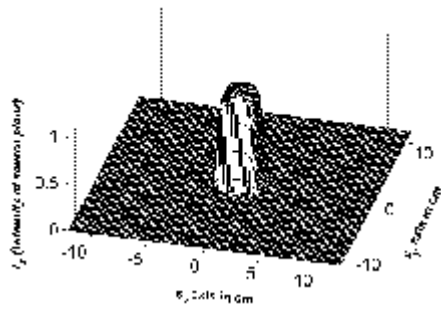


L=1.5 km

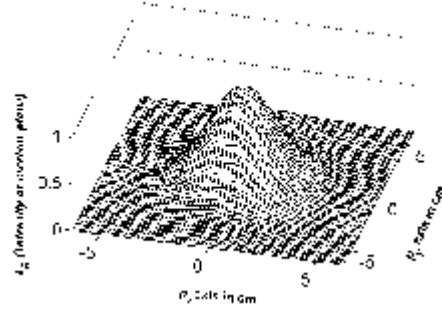


L=3 km

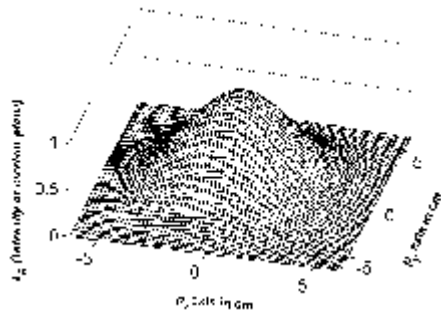
Figure 5.14: The normalized average intensity of Super gaussian beam at several propagation distances in a turbulent atmosphere with $C_n^2=10^{-14} m^{-2/3}$, $w_o=2cm$, $\lambda=632.8nm$.



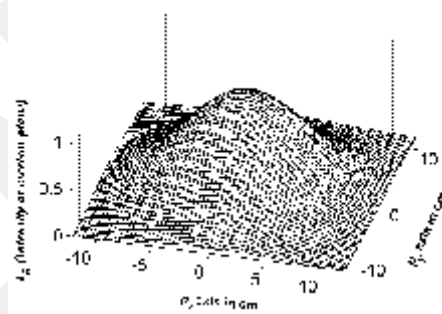
L=0 km



L=1 km

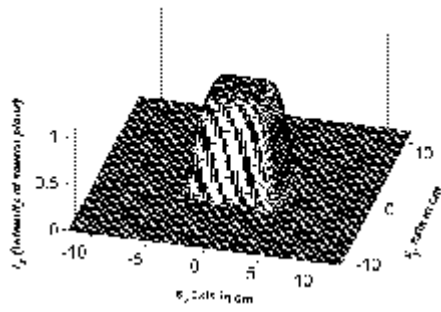


L=1.5 km

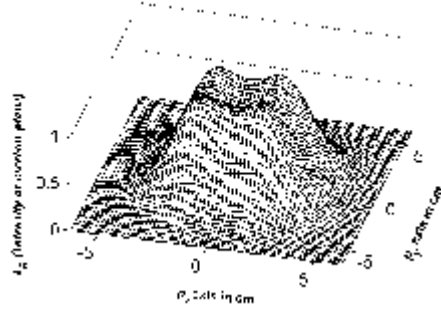


L=3 km

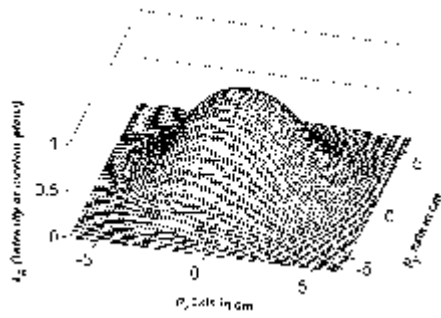
Figure 5.15: The normalized average intensity of Super gaussian beam at several propagation distances in a turbulent atmosphere with $C_n^2=10^{-14} m^{-2/3}$, $w_o=2cm$, $\lambda=1.55 \mu m$.



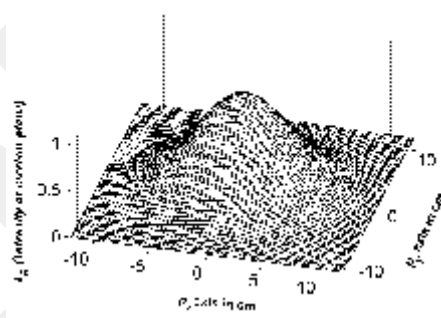
L=0 km



L=1 km



L=1.5 km



L=3 km

Figure 5.16: The normalized average intensity of Super gaussian beam at several propagation distances in a turbulent atmosphere with $C_n^2=10^{-14} m^{-2/3}$, $w_o=4cm$, $\lambda=632.8nm$.

CHAPTER 6

CONCLUSIONS

A formulation is developed to represent a general source beam to combine many types of different beams such as Bessel, Bessel Gaussian, Laguerre, Laguerre Gaussian, dark hollow, bottle, super Gaussian, Lorentz, Flat-topped. With this general source beam formulation, all the mentioned beams' source equations are obtained, compared with their existing forms in the literature and intensity patterns of some of them are plotted at the source plane.

Then, using the developed general beam formula, received average intensity is calculated in the presence of atmospheric turbulence by numerical calculation. Distributions of the average intensity patterns are obtained at the receiver plane of horizontal atmospheric links specifically for dark hollow, flat-topped, bottle, lorentz and super Gaussian beam. In our formulation, extended Huygens-Fresnel diffraction integral is used. Numerically calculated normalized average intensity distribution is plotted for each beam at different distances, wave-length, waist width of the initial beam and structure constant as quartet plots, first plot showing the intensity distribution at the source plane, the next three exhibiting the average intensity distributions at different propagation distances.

In turbulent atmosphere, dark hollow, flat-topped, bottle, lorentz and super Gaussian beam profile disappear gradually (and the central intensity increases) as propagation distance L increases. While in the far field, dark hollow, flat-topped, bottle, Lorentz and super Gaussian beams become a circular Gaussian beam in a turbulent atmosphere. This correctly checks with reference [24].

Conversion from dark hollow, flat-topped, bottle, Lorentz and super Gaussian beam to a circular Gaussian beam become quicker and the beam spot in the far field spread more rapidly for a larger structure constant.

Bottle, Lorentz and super Gaussian beam spot in the far field range spread more rapidly for longer wavelength.

GCCRIIS

REFERENCES

- [1] <http://www.mrv.com/technology/fso.php>
- [2] ERIC KOREVAAR, ISAAC I. KIM, BRUCE MCARTHUR, *Atmospheric Propagation Characteristics of Highest Importance to Commercial Free Space Optics*, MRV Communications.
- [3] <http://www.free-space-optics.org/>
- [4] SUGIANTO TRISNO (2006), *Design And Analysis Of Advanced Free Space Optical Communication Systems*, Dissertation Submitted To The Faculty Of The Graduate School Of The University Of Maryland.
- [5] SCOTT BLOOM, ERIC KOREVAAR, JOHN SCHUSTER, HEINZ WILLEBRAND (2003), *Understanding The Performance Of Free-Space Optics*, Opt. Soc. Am.,Invited.
- [6] L.C.ANDREWS (2005),*Free-Space Laser Propagation: Atmospheric Effects*,IEEE-LEOS.
- [7] ISAAC I.KIM,RON STIEGER,JOSEPH A. KOONTZ,CARTER MOURSUND,MICAHBARCLAY,PRASANNA DHIKARI,JOHN SCHUSTER,ERIC KOREVAAR, RICHARD RUIGROK, CASIMER DECUSATIS (1998), *Wireless Optical Transmission Of Fast Ethernet,FDDI, ATM, and ESCON Protocol Data Using The TerraLink Laser Communication System*, Optical Engineering, Vol. 37 No. 12.
- [8] AL NABOULSI, M., SIZUN H., DE FORNEL F., *Propagation Of Optical And Infrared Waves In The Atmosphere*, France Telecom, Université de Bourgogne.
- [9] Vikas Kukshya, *Wireless Communications*.

- [10]ANDREWS, L. C. (2005), *Laser Beam Propagation Through Random Media*, SPIE Press, Bellingham, Washington.
- [11]SERGIO JOHNSON, “*Nondiffracting*” *Light Beam*, College of Optical Sciences, University of Arizona, Tucson, Arizona 85721.
- [12]MC QUEEN, C. A., ARLT, J., DHOLAKIA K. (1999) , *An Experiment to Study A “Nondiffracting” Light Beam*, Am. J. Phys., 912-915. Vol. 67.
- [13]JORDAN, R.H., HALL, D.G. (1993), *Free-Space Azimuthal Paraxial Wave Equation: The Azimuthal Bessel-Gauss Beam Solution*, Optics Letters, 427-429. Vol. 19.
- [14]ZHANG, W., KUZYK, M.G. (2006), *Effect of a Thin Optical Kerr Medium On A Laguerre-Gaussian Beam*, Applied Physics Letters, 101103(1)-101103(3). Vol. 89.
- [15]SHARON A. KENNEDY, MATTHEW J. SZABO, HILARY TESLOW, JAMES Z. PORTERFIELD, E. R. I. ABRAHAM (2002), *Creation Of Laguerre-Gaussian Laser Modes Using Diffractive Optics*, PHYSICAL REVIEW A 66, 043801.
- [16]YANGJIAN CAI ,SAILING HE (2006), *Propagation Of Various Dark Hollow Beams In A Turbulent Atmosphere* ,Opt. Soc. Am. Vol. 14, No. 4.
- [17]MEI, Z., ZHAO, D. (2005), *Controllable Dark-Hollow Beams And Their Propagation Characteristics*, J. Opt. Soc. Am. A, 1898-1902. Vol. 22.
- [18]FREEGARDE, T., DHOLAKIA, K. (2002), *Cavity Enhanced Optical Bottle Beam As a Mechanical Amplifier*, Physical Review A., 013413. Vol. 66.
- [19]HALİL TANYER EYYUBOĞLU, ÇAĞLAR ARPALI, YAHYA BAYKAL (2006), *Flat Topped Beams And Their Characteristics in Turbulent Media*, OPTICS EXPRESS Vol. 14, No. 10.

- [20] A BULLETIN OF THE INDIAN LASER ASSOCIATION 2007, *Special Issue on Best Theses and Posters at National Laser Symposium – 2006*, Vol. 18, No.1.
- [21] GAWHARY, O.E., SEVERINI, S. (2006), *Lorentz Beams*, J. Opt. A: Pure Appl. Opt., 409. Vol. 8.
- [22] ARPALI ÇAĞLAR. CANAN YAZICIOĞLU, HALİL TANYER EYYUBOĞLU, SERAP ALTAY ARPALI, YAHYA BAYKAL. (2006), *Simulator for General-Type Beam Propagation in Turbulent Atmosphere*, Opt. Express, 8918-8928, Vol. 14.
- [23] YANGJIAN CAI ,SAILING HE (2006), *Propagation Of Various Flat-Topped Beams In A Turbulent Atmosphere* ,J. Opt. A: Pure Appl. Opt. 8(2006) 537-545.
- [24] HALİL TANYER EYYUBOĞLU, YAHYA BAYKAL, EMRE SERMUTLU. (2006), *Convergence Of General Beams Into Gaussian Intensity Profiles After Propagation In Turbulent Atmosphere*, Optcom, 265(2006) 399-405.


```

variable_1=A1.*Tr.*((P.*(sx.^2+sy.^2).^gama1+R.*(sx.^2+sy.^2).^gama2).^gama3).
...
./(((d1.*alfasxl.^2+d3.*sx.^2).^c1).*(d2.*alfasy1.^2+d4.*sy.^2).^c2);
V=(B-C.*exp(-D.*(sx./alfasxl).^f1).^F1-M.*sx.*sy-E.*(sy./alfasy1).^f2).^F2)...
-G.*exp(-H.*(sx./alfasxl).^F4-J.*(sy./alfasy1).^F5-(j.*m2.*phi)).^F3;
variable_2=(A-V).*exp(-j.*(Vxl.*sx+Vyl.*sy));
% variable_3=H(n,ax*sx+bx).*H(m,ay*sy+by)
u_s=u_s+variable_1.*variable_2; %.*variable_3

end

```

```

I_CB = u_s.* conj(u_s) ;
maxsinh = max(max(I_CB));
I_CB = I_CB / maxsinh;
meshc(sxn,syn,real(I_CB));
view([14.5 56.0]); colormap([0 0 0]);
xlabel('\its_x\rm\bf axis in cm',FontSize,12,FontWeight,'bold');
ylabel('\its_y\rm\bf axis in cm',FontSize,12,FontWeight,'bold',Rotation,26)
zlabel('\fontname{Times}\fontsize{14}\itI_s (Intensity at source
plane)',FontSize,12,FontWeight,'bold')
set(gcf,'Renderer','Zbuffer');set(gcf,'Color','w');set(gca,FontSize,16);
set(gcf,'Renderer','Zbuffer');set(gcf,'Color','w');set(gca,FontSize,16);
axis ([min(min(sxn))*1 max(max(sxn))*1 min(min(syn))*1 max(max(syn))*1 0 1])
pause;clf reset

```



```

maxsinh = max(max(I_CB)); %I_CB nin en büyük terimi saptanıyor burda aslında
I_CB = I_CB / maxsinh;%I_CB nin tüm değerleri en büyük terime bölünüyor
böylece I_CB değerleri 0-1 aralığında değişiyor
meshc(sxn,syn,real(I_CB));
view([14.5 56.0]); colormap([0 0 0]);
xlabel('\its_x\rm\bf axis in cm','FontSize',12,'FontWeight','bold','Rotation',-5);
ylabel('\its_y\rm\bf axis in cm','FontSize',12,'FontWeight','bold','Rotation',65)
zlabel('\fontname{Times}\fontsize{14}\itI_s_N (Intensity at source
plane)','FontSize',12,'FontWeight','bold')
set(gcf,'Renderer','Zbuffer');set(gcf,'Color','w');set(gca,'FontSize',16);
axis ([min(min(sxn)) max(max(sxn)) min(min(syn)) max(max(syn)) 0 1])
pause;clf reset

```

```

function y = funb(a,b)
y = factorial(a)/factorial(b)/factorial(a-b);
function y = funT(e1)
T = 1;
for j = 1:e1
    T = (2*j-1)*T;
end
y = T;
function yout = H(nn,xx)
mat = cat(4,ones(size(xx)),2*xx,4*xx.^2-2);
for say = 4:nn+1
    mat(:, :, say) = 2*xx.*mat(:, :, say-1) - 2*(say-2)*mat(:, :, say-2);
end
yout = mat(:, :, nn+1);

```



```

I_CB = u_s.*conj(u_s);
maxsinh = max(max(I_CB));
I_CB = I_CB / maxsinh;
meshc(sxn,syn,real(I_CB)); view([14.5 56.0]); colormap([0 0 0]);
xlabel('\its_x\rm\bf axis in cm', 'FontSize', 12, 'FontWeight', 'bold', 'Rotation', -5);
ylabel('\its_y\rm\bf axis in cm', 'FontSize', 12, 'FontWeight', 'bold', 'Rotation', 65);
zlabel('\fontname{Times}\fontsize{14}\itI_s (Intensity at source plane)', 'FontSize', 12, 'FontWeight', 'bold');
set(gcf, 'Renderer', 'Zbuffer'); set(gcf, 'Color', 'w'); set(gca, 'FontSize', 16);
axis ([min(min(sxn))*1 max(max(sxn))*1 min(min(syn))*1 max(max(syn))*1 0 1]);
pause; clf reset

```

GCRIS


```

I_CB = u_s.*conj(u_s);
maxsinh = max(max(I_CB));
I_CB = I_CB / maxsinh;
meshc(sxn,syn,real(I_CB)); view([14.5 56.0]); colormap([0 0 0]);
xlabel('\its_x\rm\bf axis in cm',FontSize,12,FontWeight,'bold',Rotation,-5);
ylabel('\its_y\rm\bf axis in cm',FontSize,12,FontWeight,'bold',Rotation,65);
zlabel('\fontname{Times}\fontsize{14}\itI_s (Intensity at source
plane)',FontSize,12,FontWeight,'bold');
set(gcf,'Renderer','Zbuffer');set(gcf,'Color','w');set(gca,'FontSize',16);
axis ([min(min(sxn))*1 max(max(sxn))*1 min(min(syn))*1 max(max(syn))*1 0 1]);
pause;clf reset

```

GCRIS


```
meshc(sxn,syn,real(I_CB)); view([14.5 56.0]); colormap([0 0 0]);
xlabel('\its_x\rm\bf axis in cm','FontSize',12,'FontWeight','bold','Rotation',-5);
ylabel('\its_y\rm\bf axis in cm','FontSize',12,'FontWeight','bold','Rotation',65);
zlabel('\fontname{Times}\fontsize{14}\itI_s (Intensity at source
plane)','FontSize',12,'FontWeight','bold');
set(gcf,'Renderer','Zbuffer');set(gcf,'Color','w');set(gca,'FontSize',16);
axis ([min(min(sxn))*1 max(max(sxn))*1 min(min(syn))*1 max(max(syn))*1 0 1]);
pause;clf reset
```

GCPRIS


```

view([14.5 56.0]); colormap([0 0 0]);
xlabel('\its_x\rm\bf axis in cm','FontSize',12,'FontWeight','bold','Rotation',-5);
ylabel('\its_y\rm\bf axis in cm','FontSize',12,'FontWeight','bold','Rotation',65)
zlabel('\fontname{Times}\fontsize{14}\itI_s_N (Intensity at source
plane)','FontSize',12,'FontWeight','bold')
set(gcf,'Renderer','Zbuffer');set(gcf,'Color','w');set(gca,'FontSize',16);
axis ([min(min(sxn)) max(max(sxn)) min(min(syn)) max(max(syn)) 0 1])
pause;clf reset

```

```

% function yout = H(nn,xx)
% n = nn + 1;ary = [];
% [row,col] = size(xx);yout = [];
% for rowk = 1:row
%   y = [];
%   for colk = 1:col
%     x = xx(rowk,colk);
% h(1) = 1; h(2) = x*2;
% yy = h(1);
% if nn ~= 0
%   yy = h(2);
%   if nn ~= 1
%     for j = 3:n
%       h(j) = 2*x*h(j-1) - 2*(j-2)*h(j-2);
%     end
%     yy = h(j);
%   end
% end
% y = [y yy];
% end
% yout(rowk,:) = y;
% end

```



```
I_CB = I_CB / maxsinh;
meshc(sxn,syn,real(I_CB)); view([14.5 56.0]); colormap([0 0 0]);
xlabel('\its_x\rm\bf axis in cm','FontSize',12,'FontWeight','bold','Rotation',-5);
ylabel('\its_y\rm\bf axis in cm','FontSize',12,'FontWeight','bold','Rotation',65);
zlabel('\fontname{Times}\fontsize{14}\itI_s (Intensity at source
plane)','FontSize',12,'FontWeight','bold');
set(gcf,'Renderer','Zbuffer');set(gcf,'Color','w');set(gca,'FontSize',16);
axis ([min(min(sxn))*1 max(max(sxn))*1 min(min(syn))*1 max(max(syn))*1 0 1]);
pause;clf reset
```

GCPRIS


```
maxsinh = max(max(I_CB));
I_CB = I_CB / maxsinh;
meshc(sxn,syn,real(I_CB)); view([14.5 56.0]); colormap([0 0 0]);
xlabel('\its_x\rm\bf axis in cm', 'FontSize', 12, 'FontWeight', 'bold', 'Rotation', -5);
ylabel('\its_y\rm\bf axis in cm', 'FontSize', 12, 'FontWeight', 'bold', 'Rotation', 65);
zlabel('\fontname{Times}\fontsize{14}\itI_s (Intensity at source
plane)', 'FontSize', 12, 'FontWeight', 'bold');
set(gcf, 'Renderer', 'Zbuffer'); set(gcf, 'Color', 'w'); set(gca, 'FontSize', 16);
axis ([min(min(sxn))*1 max(max(sxn))*1 min(min(syn))*1 max(max(syn))*1 0 1]);
pause; clf reset
```

GCPRIS


```
xlabel('\its_x\rm\bf axis in cm','FontSize',12,'FontWeight','bold','Rotation',-5);
ylabel('\its_y\rm\bf axis in cm','FontSize',12,'FontWeight','bold','Rotation',65)
xlabel('\fontname{Times}\fontsize{14}\itI_s_N (Intensity at source
plane)','FontSize',12,'FontWeight','bold')
set(gcf,'Renderer','Zbuffer');set(gcf,'Color','w');set(gca,'FontSize',16);
axis ([min(min(sxn)) max(max(sxn)) min(min(syn)) max(max(syn)) 0 1])
pause;clf reset
```

GCPRIS

```

function save _darkhollow
clear;clc;clf;warning off MATLAB:divideByZero;close all;clear global
global lamda k alfasxarr alfasyarr Vxarr Vyarr narr marr axarr ayarr bxarr byarr L
Cn ro2 px py
lamda = 632.8e-9; k = 2*pi/lamda;
alfasxarr = [sqrt(2).*1e-2 sqrt(2).*1e-2 sqrt(2).*1e-2 sqrt(2).*1e-2 sqrt(2).*1e-2
sqrt(2e-4) sqrt(2e-4) sqrt(2e-4) sqrt(2e-4) sqrt(2e-4) sqrt(2e-4) sqrt(2e-4) sqrt(2e-4)
sqrt(2e-4) sqrt(2e-4) sqrt(2e-4) sqrt(2e-4) sqrt(2e-4) sqrt(2e-4) sqrt(2e-4) ];
alfasyarr = alfasxarr;
Vxarr = [0 0 0 0 0 0 0 0 0 0 0 0 0 0 0 0 0 0 0 0 0 0]; Vyarr = Vxarr;
narr = [0 0 0 0 0 0 0 0 0 0 0 0 0 0 0 0 0 0 0 0 0 0]; marr = narr;
axarr = 1./alfasxarr;%formül
ayarr = 1./alfasyarr;
bxarr = 0.*axarr; byarr = 0.*ayarr;
Cn = 1e-14;L = 5000;
ro2 = (0.545*Cn*k^2*L)^(-1.2);
alt = -5e-2;ust =5e-2;
pxsetn = -32e-2:10e-3:32e-2;pysetn = pxsetn;
length(pxsetn)

tic

I_rarr = [];

for ipy = 1:length(pysetn)
    I_rrow=[];
    py= pysetn(ipy);

for ipx = 1:length(pxsetn)
    px=pxsetn(ipx);
    res1 = azhizlifourquade(@funt1,alt,ust,alt,ust,alt,ust,alt,ust);

    I_rrow = [I_rrow res1];
    size(I_rrow);
end
    I_rarr = [I_rarr;I_rrow];
end

[px,py]=meshgrid(pxsetn,pysetn);
pxn=px/1e-2;pyn=py/1e-2;
format short e;

I_rarr= real(I_rarr);

save('darkhollowcai_cn14_5km','I_rarr','-ascii')
toc
t=toc/3600

```

```

function yt = funt1(sx1,sx2,sy1,sy2)
global lamda k alfasxarr alfasyarr Vxarr Vyarr narr marr axarr ayarr bxarr byarr L
Cn ro2 px py
mi=0;f=1;N=3;
crosscarpim=0;

for l1=1:N
    for l2=1:N
        ksi2=l2;
        A12=(-1).^(ksi2-1).*factorial(N)/(N.*factorial(ksi2).*factorial(N-ksi2));
        Tr=1;gama3=0;c1=0;c2=0;A=0;B=0;
        C=1;D=ksi2./2;G=-1;mi=0;E=ksi2./2;epsilon=0.9486832;
        H=ksi2./(2.*epsilon.^2);F1=2;F2=2;F3=1;F4=2;
        J=ksi2./(2.*epsilon.^2);F5=2;m2=0;
        f1=1;f2=1;
        M=0;
        %s2=(sx2.^2+sy2.^2)^(1./2);

        alfasx12=alfasxarr(l2);alfasy12=alfasyarr(l2);
        ax2 = axarr(l2); ay2 = ayarr(l2);
        bx2 = bxarr(l2); by2= byarr(l2);
        Vx12 = Vxarr(l2); Vy12 = Vyarr(l2);
        n2 = narr(l2); m2 = marr(l2);
        %şimdide tezde tanımlanmamış parametreleri tanımlayalım
        P=0;gama1=0;R=0;gama2=0;d1=0;d2=0;phi=0;

        variable_1=conj(A12).*Tr.*((P.*(sx2.^2+sy2.^2).^gama1+R.*(sx2.^2+sy2.^2).^gama
        2).^gama3)...
        ./(((d1.*alfasx12.^2+sx2.^2).^c1).*(d2.*alfasy12.^2+sy2.^2).^c2);
        V2=(B-C.*exp(-D.*(sx2./(alfasx12).^f1).^F1-E.*(sy2./(alfasy12).^f2).^F2)...
        -G.*exp(-H.*(sx2./alfasx12).^F4-J.*(sy2./alfasy12).^F5+(j.*m2.*phi))).^F3;
        variable_2=(A-V2).*exp(+j.*(Vx12.*sx2+Vy12.*sy2));
        %variable_3=H(n2,ax2*sx2+bx2).*H(m2,ay2*sy2+by2)
        u_s2=variable_1.*variable_2; %.*variable_3

        ksi1=l1;
        A11=(-1).^(ksi1-1).*factorial(N)/(N.*factorial(ksi1).*factorial(N-ksi1));
        Tr=1;gama3=0;c1=0;c2=0;A=0;B=0;
        C=1;D=ksi1./2;G=-1;mi=0;E=ksi1./2;epsilon=0.9486832;
        H=ksi1./(2.*epsilon.^2);F1=2;F2=2;F3=1;F4=2;
        J=ksi1./(2.*epsilon.^2);F5=2;m2=0;
        f1=1;f2=1;
        M=0;
        %s1=(sx1.^2+sy1.^2)^(1./2);

```

```

alfasx1=alfasxarr(11);alfasy1=alfasyarr(11);
ax1 = axarr(11); ay1 = ayarr(11);
bx1 = bxarr(11); by1= byarr(11);
Vx11 = Vxarr(11); Vyl1 = Vyarr(11);
n1 = narr(11); m1 = marr(11);
%şimdide tezde tanımlanmamış parametreleri tanımlayalım
P=0;gama1=0;R=0;gama2=0;d1=0;d2=0;phi=0;

variable_3=A11.*Tr.*((P.*(sx1.^2+sy1.^2).^gama1+R.*(sx1.^2+sy1.^2).^gama2).^gama3)...
./(((d1.*alfasx11.^2+sx1.^2).^c1).*(d2.*alfasy11.^2+sy1.^2).^c2);
V1=(B-C.*exp(-D.*(sx1./alfasx11).^f1).^F1-E.*(sy1./alfasy11).^f2).^F2)...
-G.*exp(-H.*(sx1./alfasx11).^F4-J.*(sy1./alfasy11).^F5-(j.*m2.*phi)).^F3;
variable_4=(A-V1).*exp(-j.*(Vx11.*sx1+Vyl1.*sy1));
% variable_5=H(n1,ax1*sx1+bx1).*H(m1,ay1*sy1+by1)
u_s1=variable_3.*variable_4;%.*variable_5

crosscarpim=crosscarpim+u_s2.*u_s1;
end
end

yt = (crosscarpim).* ...
exp(0.5*j*k*(sx1.^2 - 2*px*sx1 - sx2.^2 + 2*px*sx2)/L).*exp(0.5*j*k*(sy1.^2 -
2*py*sy1 - sy2.^2 + 2*py*sy2)/L).* ...
exp(-(sx1.^2 - 2*sx1.*sx2 + sx2.^2)/ro2).*exp(-(sy1.^2 - 2*sy1.*sy2 +
sy2.^2)/ro2);

function yout = H(nn,xx)
mat = cat(4,ones(size(xx)),2*xx,4*xx.^2-2);
for say = 4:nn+1
mat(:, :, :, say) = 2*xx.*mat(:, :, :, say-1) - 2*(say-2)*mat(:, :, :, say-2);
end
yout = mat(:, :, :, nn+1);

```



```

I_rarr
size(I_rarr)

save('bottlealldata','I_rarr','-ascii')
toc
t=toc/3600

function yt = funt1(sx1,sx2,sy1,sy2)
global lamda k alfasxarr alfasyarr Vxarr Vyarr narr marr axarr ayarr bxarr byarr L
Cn ro2 px py
mi=0;f=1;N=1;
crosscarpim=0;

for l1=1:N
    for l2=1:N

alfasx12=alfasxarr(l2);alfasy12=alfasyarr(l2);
ax2 = axarr(l2); ay2 = ayarr(l2);
bx2 = bxarr(l2); by2= byarr(l2);
Vx12 = Vxarr(l2); Vyl2 = Vyarr(l2);
n2 = narr(l2); m2 = marr(l2);
M=0;

N=1;A12=1;Tr=1;c1=0;c2=0;P=-1./(2.*alfasx12.^4);
gama1=2;R=2./alfasy12.^2;gama2=1;gama3=1;
A=0;B=0;C=1;D=1./2;E=1./2;G=0;
f1=1;f2=1;F1=2;F2=2;F3=1;

d1=0;d2=0;H=0;F4=0;J=0;F5=0;m2=0;phi=0;
d3=0;d4=0;

variable_1=conj(A12).*Tr.*((P.*(sx2.^2+sy2.^2).^gama1+R.*(sx2.^2+sy2.^2).^gama
2).^gama3)...
./(((d1.*alfasx12.^2+sx2.^2).^c1).*(d2.*alfasy12.^2+sy2.^2).^c2);
V2=(B-C.*exp(-D.*(sx2./(alfasx12).^f1).^F1-E.*(sy2./(alfasy12).^f2).^F2)...
-G.*exp(-H.*(sx2./alfasx12).^F4-J.*(sy2./alfasy12).^F5+(j.*m2.*phi)).^F3;
variable_2=(A-V2).*exp(+j.*(Vx12.*sx2+Vyl2.*sy2));
% variable_3=H(n2,ax2*sx2+bx2).*H(m2,ay2*sy2+by2)
u_s2=variable_1.*variable_2; %.*variable_3

alfasx11=alfasxarr(l1);alfasy11=alfasyarr(l1);
ax1 = axarr(l1); ay1 = ayarr(l1);
bx1 = bxarr(l1); by1= byarr(l1);
Vx11 = Vxarr(l1); Vyl1 = Vyarr(l1);
n1 = narr(l1); m1 = marr(l1);
M=0;

```

```

N=1;A11=1;Tr=1;c1=0;c2=0;P=-1./(2.*alfasx11.^4);
gama1=2;R=2./alfasy11.^2;gama2=1;gama3=1;
A=0;B=0;C=1;D=1./2;E=1./2;G=0;
f1=1;f2=1;F1=2;F2=2;F3=1;

```

```

d1=0;d2=0;H=0;F4=0;J=0;F5=0;m2=0;phi=0;
d3=0;d4=0;

```

```

variable_3=A11.*Tr.*((P.*(sx1.^2+sy1.^2).^gama1+R.*(sx1.^2+sy1.^2).^gama2).^gama3)...

```

```

./(((d1.*alfasx11.^2+sx1.^2).^c1).*(d2.*alfasy11.^2+sy1.^2).^c2);
V1=(B-C.*exp(-D.*(sx1./alfasx11).^f1).^F1-E.*(sy1./alfasy11).^f2).^F2)...
-G.*exp(-H.*(sx1./alfasx11).^F4-J.*(sy1./alfasy11).^F5-(j.*m2.*phi)).^F3;
variable_4=(A-V1).*exp(-j.*(Vx11.*sx1+Vy11.*sy1));
%variable_5=H(n1,ax1*sx1+bx1).*H(m1,ay1*sy1+by1)
u_s1=variable_3.*variable_4;%.*variable_5

```

```

crosscarpim=crosscarpim+u_s2.*u_s1;

```

```

end
end

```

```

yt = (crosscarpim).* ...
exp(0.5*j*k*(sx1.^2 - 2*px*sx1 - sx2.^2 + 2*px*sx2)/L).*exp(0.5*j*k*(sy1.^2 -
2*py*sy1 - sy2.^2 + 2*py*sy2)/L).* ...
exp(-(sx1.^2 - 2*sx1.*sx2 + sx2.^2)/ro2).*exp(-(sy1.^2 - 2*sy1.*sy2 +
sy2.^2)/ro2);

```

```

function yout = H(nn,xx)
mat = cat(4,ones(size(xx)),2*xx,4*xx.^2-2);
for say = 4:nn+1
mat(:, :, :, say) = 2*xx.*mat(:, :, :, say-1) - 2*(say-2)*mat(:, :, :, say-2);
end
yout = mat(:, :, :, nn+1);

```



```

size(I_rarr)

save('LORENTZalldata','I_rarr','-ascii')
toc
t=toc/3600

function yt = funt1(sx1,sx2,sy1,sy2)
global lamda k alfasxarr alfasyarr Vxarr Vyarr narr marr axarr ayarr bxarr byarr L
Cn ro2 px py
mi=0;f=1;N=1;
crosscarpim=0;

for l1=1:N
    for l2=1:N
alfasx12=alfasxarr(l2);alfasy12=alfasyarr(l2);
ax2 = axarr(l2); ay2 = ayarr(l2);
bx2 = bxarr(l2); by2= byarr(l2);
Vx12 = Vxarr(l2); Vyl2 = Vyarr(l2);
n2 = narr(l2); m2 = marr(l2);

E0=1;A12=2.*E0.*alfasx12.*alfasy12;Tr=1;gama3=0;c1=1;c2=1;
d1=2;d2=2;A=2;F3=0;
n=0;m=0;
M=0;d3=1;d4=1;
%tezde geçen parametrelere değer atadım yukarda

gama1=0;gama2=0;R=0;P=0;B=0;
C=0;D=0;E=0;f1=0;F1=0;f2=0;E=0;F2=0;G=0;H=0;F4=0;J=0;F5=0;m2=0;phi=0;

variable_1=conj(A12).*Tr.*((P.*(sx2.^2+sy2.^2).^gama1+R.*(sx2.^2+sy2.^2).^gama
2).^gama3)....
./(((d1.*alfasx12.^2+sx2.^2).^c1).*(d2.*alfasy12.^2+sy2.^2).^c2);
V2=(B-C.*exp(-D.*(sx2./(alfasx12).^f1).^F1-E.*(sy2./(alfasy12).^f2).^F2)...
-G.*exp(-H.*(sx2./alfasx12).^F4-J.*(sy2./alfasy12).^F5+(j.*m2.*phi))).^F3;
variable_2=(A-V2).*exp(+j.*(Vx12.*sx2+Vyl2.*sy2));
% variable_3=H(n2,ax2*sx2+bx2).*H(m2,ay2*sy2+by2)
u_s2=variable_1.*variable_2; %.*variable_3

alfasx11=alfasxarr(l1);alfasy11=alfasyarr(l1);
ax1 = axarr(l1); ay1 = ayarr(l1);
bx1 = bxarr(l1); by1= byarr(l1);
Vx11 = Vxarr(l1); Vyl1 = Vyarr(l1);
n1 = narr(l1); m1 = marr(l1);

E0=1;A11=2.*E0.*alfasx11.*alfasy11;Tr=1;gama3=0;c1=1;c2=1;
d1=2;d2=2;A=2;F3=0;
n=0;m=0;
M=0;d3=1;d4=1;

```

```

gama1=0;gama2=0;R=0;P=0;B=0;
C=0;D=0;E=0;f1=0;F1=0;f2=0;E=0;F2=0;G=0;H=0;F4=0;J=0;F5=0;m2=0;phi=0;

variable_3=A11.*Tr.*((P.*(sx1.^2+sy1.^2).^gama1+R.*(sx1.^2+sy1.^2).^gama2).^gama3)...
./(((d1.*alfasx11.^2+sx1.^2).^c1).*(d2.*alfasy11.^2+sy1.^2).^c2);
V1=(B-C.*exp(-D.*(sx1./alfasx11).^f1).^F1-E.*(sy1./alfasy11).^f2).^F2)...
-G.*exp(-H.*(sx1./alfasx11).^F4-J.*(sy1./alfasy11).^F5-(j.*m2.*phi)).^F3;
variable_4=(A-V1).*exp(-j.*(Vx11.*sx1+Vy11.*sy1));
% variable_5=H(n1,ax1*sx1+bx1).*H(m1,ay1*sy1+by1)
u_s1=variable_3.*variable_4;%.*variable_5

crosscarpim=crosscarpim+u_s2.*u_s1;
end
end

yt = (crosscarpim).* ...
exp(0.5*j*k*(sx1.^2 - 2*px*sx1 - sx2.^2 + 2*px*sx2)/L).*exp(0.5*j*k*(sy1.^2 -
2*py*sy1 - sy2.^2 + 2*py*sy2)/L).* ....
exp(-(sx1.^2 - 2*sx1.*sx2 + sx2.^2)/ro2).*exp(-(sy1.^2 - 2*sy1.*sy2 +
sy2.^2)/ro2);

function yout = H(nn,xx)
mat = cat(4,ones(size(xx)),2*xx,4*xx.^2-2);
for say = 4:nn+1
mat(:, :, say) = 2*xx.*mat(:, :, say-1) - 2*(say-2)*mat(:, :, say-2);
end
yout = mat(:, :, nn+1);

```